Supporting Information

Understanding Förster Resonance Energy Transfer in the Sheet Regime with DNA Brick-Based Dye Networks

Divita Mathur,[1,4,#] Anirban Samanta,[1,4,7,#] Mario G. Ancona,[2#*] Sebastián A. Díaz,[1]

Youngchan Kim,[3] Joseph S. Melinger,[2] Ellen R. Goldman,[1]

John Paul Sadowski,[1,5] Luvena L. Ong,[6,8] Peng Yin,[6] and Igor L. Medintz[1*]

[1]Center for Bio/Molecular Science and Engineering Code 6900
[2]Electronic Science and Technology Division Code 6800
[3]Center for Materials Physics and Technology Code 6390
U.S. Naval Research Laboratory
Washington, D.C. 20375 USA

[4]College of Science
George Mason University
Fairfax, VA 22030 USA

[5]American Society for Engineering Education
Washington, D.C. 20001 USA

[6]Wyss Institute for Biologically Inspired Engineering
Harvard University
Boston, MA 02115 USA

[7]Current Address: Ramakrishna Mission Vidyamandira, Belur Math,
Howrah 711202, India

[8]Current Address: Janssen Pharmaceuticals
Raritan, NJ 08869 USA

[#]Authors contributed equally

*Email: Igor.Medintz@nrl.navy.mil; Mario.Ancona@nrl.navy.mil

Table of contents:

DNA Block Design Diagrams, Characterization, and Strands

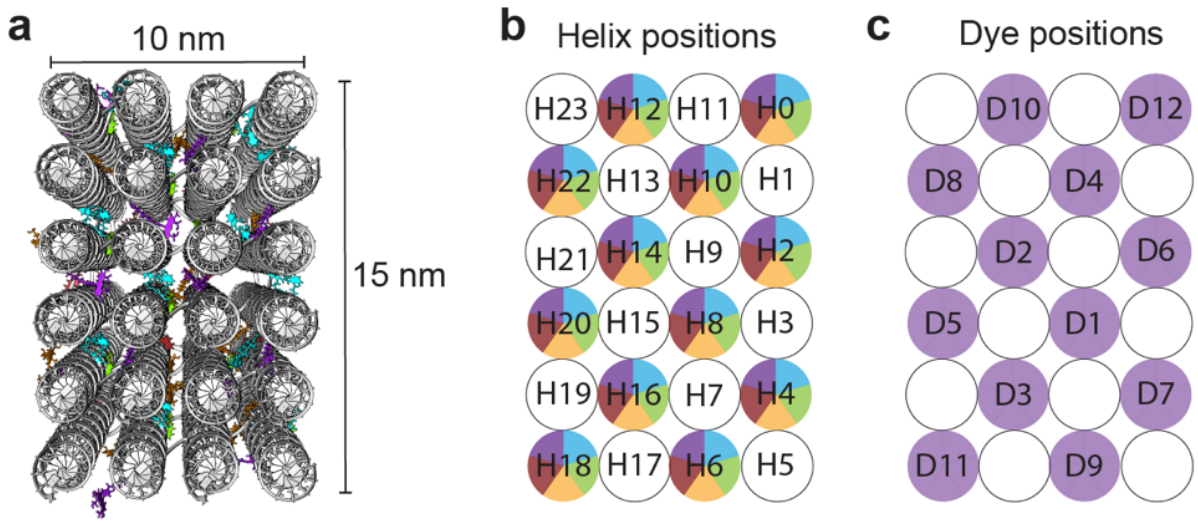

Figure S1: Schematic of the DNA block and dye placement. (a) Front view of the DNA block highlighting the 6×4 helix bundles that run the length of the structure. **(b)** Helix numbering scheme with colored circles indicating helices where dyes are tethered. **(c)** Nomenclature designating dye attachment positions on the helices, these are numbered in the order in which dyes were incorporated into experimental assemblies when increasing from 1 up to 12. Note, D followed by an integer as in D12 indicates a dye position, all other instances of the letter D indicate the word 'donor' unless otherwise stated.

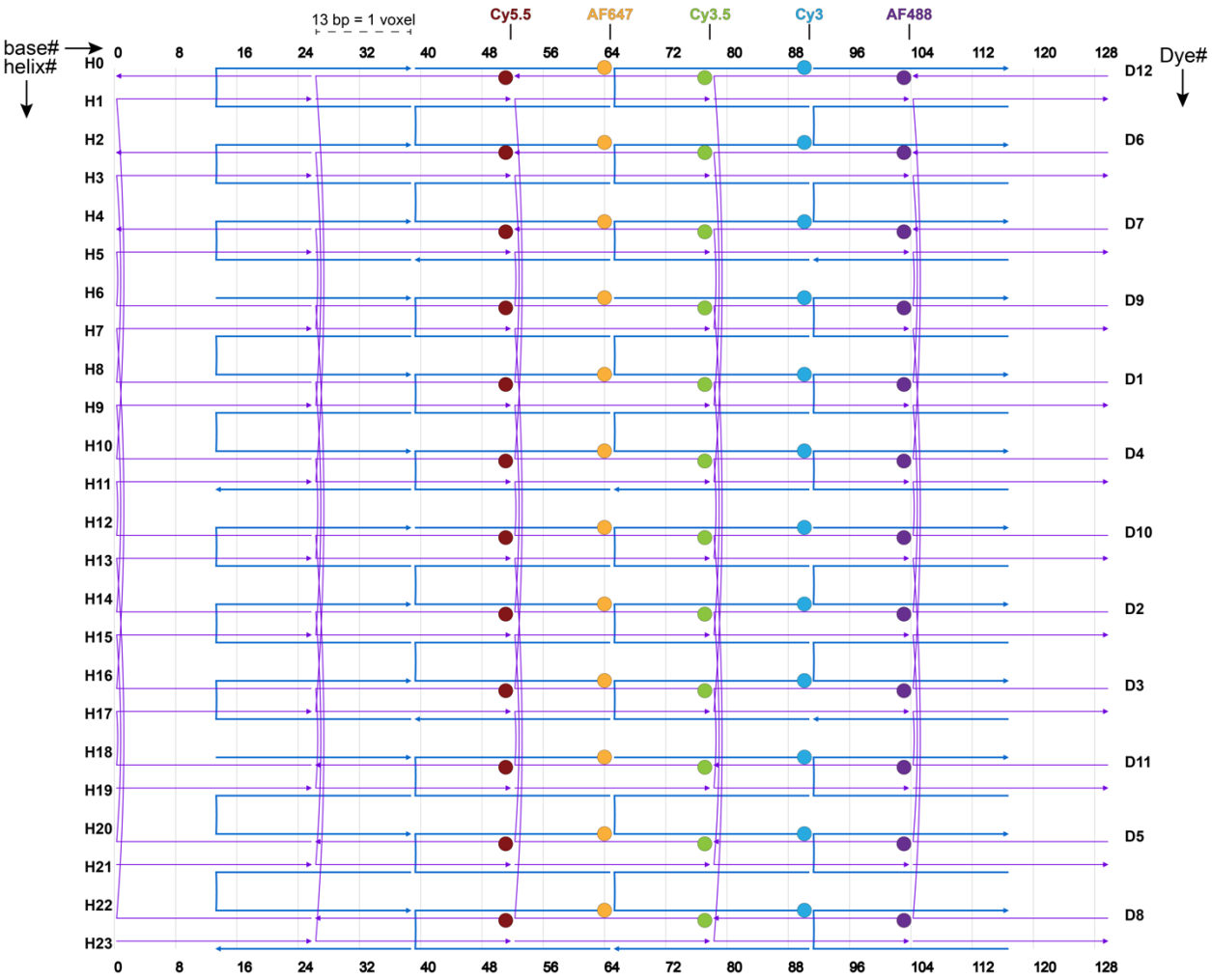

Figure S2: DNA strand diagram of the cuboidal Block structure. DNA strands are represented in blue and purple. Numbers on the four sides of the diagram represent helix numbers (*left*), base number (*top/bottom*), and dye number (*right*). Colored circles indicate location of AF488 (*violet*), Cy3 (*blue*), Cy3.5 (*green*), AF647 (*orange*), and Cy5.5 (*maroon*).

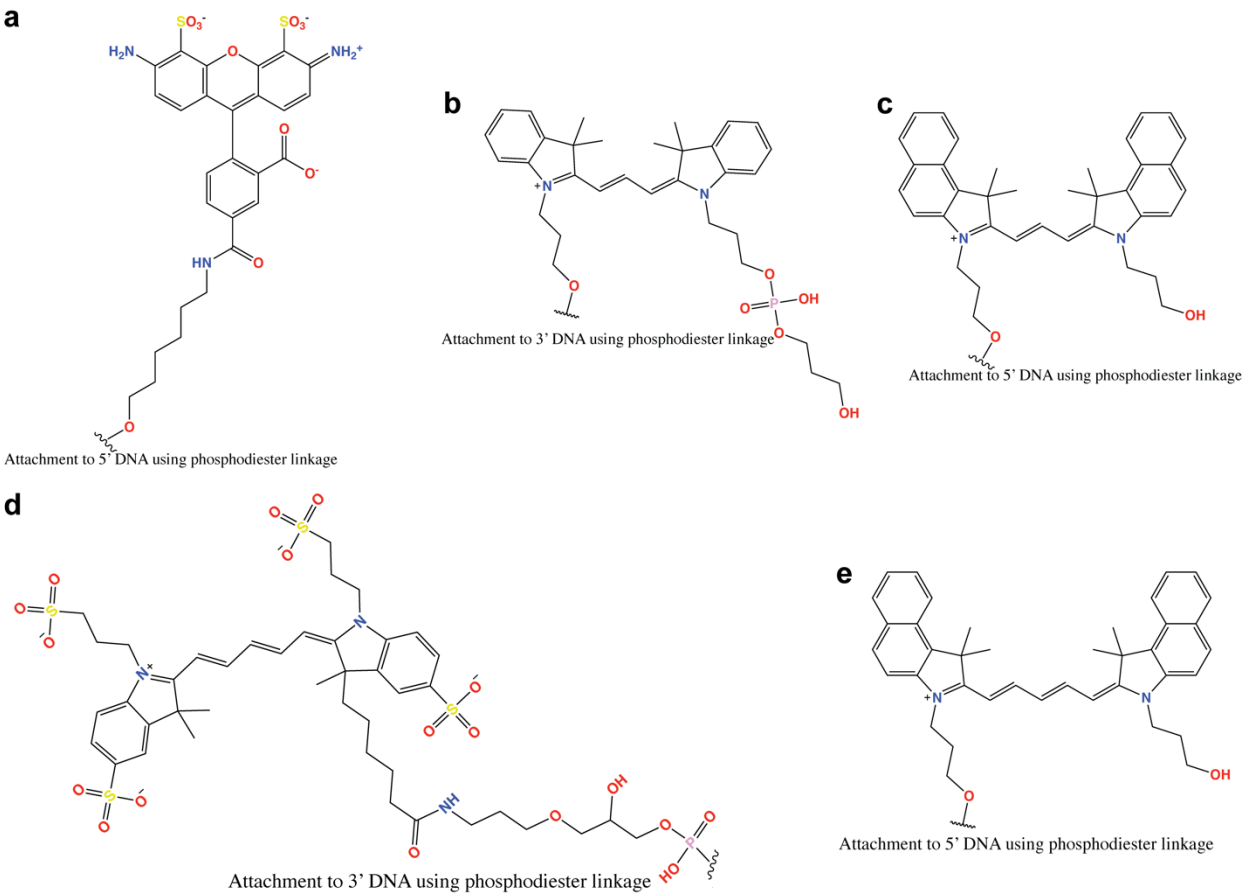

Figure S3: Structure of the dye molecules and their corresponding DNA attachment chemistries. (a) Alexa Fluor 488, **(b)** Cy3**, (c)** Cy3.5, **(d)** Alexa Fluor 647, **(e)** Cy5.5.

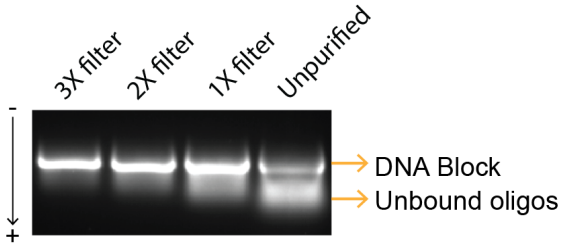

Figure S4: Characterization of DNA block purification *via* agarose gel electrophoresis. Representative agarose gel electropherogram (2% agarose gel in 1×TBE buffer, 89 mM Tris-borate and 2 mM EDTA, pH 8.3) showing purification of the assembled DNA block from unbound brick strands with 3 consecutive rounds of purification using Amicon 100 kDa size-exclusion filtration columns.

Table S1: DNA Block sequences. Dye modified strands are listed after the un-labeled versions. In dye-modified oligos, the end base is replaced with the corresponding dye. Dye-labeled strands have background shading corresponding to the dye colors used in the main manuscript and SI. Strand notation of "X" and "Y" represents the designated blue-colored and purple-colored strands in the caDNAno design of Figure S2, respectively. However, in case of the DNA block it bears no relevance.

Name	Sequence	Start
X00	CCGCGGACGAATTGTGAAAAATTCAA	[0, 39]
X01	TCATTGCTACCTAACGGCTAACACCC	[0, 91]
X02	CGCGAACTTTCCTTATCAATCGTATTTGACCGCTGAGTGTGTGCAAATGCCT	[1, 38]
X03	TGCCTGCATCCCGCCTCTTATTGGATACGACCTACTAGCTATAGACTGGTAC	[1, 90]
X04	TATGAGGGAAGGACCCTTGCGATTCTTTCTGCACGAGTAAGAATACTCGATT	[1, 64]
X05	TGAAAGCCAAGTGTAGGGCCGATTGGACAACGGTATATAACGCCCGAAGGGG	[1, 116]
X06	CGGTCCGATTCCCGGAACTGTCGCAGATCCGAGTCTTGACCTCGGTATTCAC	[3, 38]
X07	TCCCGATCAAAGGTCATCCGGTAATCTCGCATTGGTCTAAGTCGTAAAGAAA	[3, 90]
X08	TCTACCCGTGCTTCGATGCACAATGGACCGTCGCACGACGCTGCCTCAGCAT	[3, 64]
X09	CTGCCACAGACCGGGCCCAGTTAAGGAGGATGAAGTCTTAGCGGCCGGTTTC	[3, 116]
X10	TTCCAGAAGCAATAGACGTGTCAGTTAAAGATTTGAGGGTATGTGCGGGTCT	[5, 38]
X11	CCCAGTCCGAACGGGGGCTTGTGCGCAGTAGCCCTTGAAAGCTGGGCTATAA	[5, 90]
X12	GAACGCTTCAGGGAGTTGGTCATCCT	[5, 64]
X13	TACTGCCTTGGGCAATTCCTATAAGT	[5, 116]
X14	CAATACTTAGGGAGCGAATCCGAGAA	[6, 13]
X15	CGCCAGGAACCATATTGCGGTCCAAT	[6, 65]
X16	GGTTTTGTTCAAGCTGCGCTTGGCACCAGATTATGAGCACGTGCGGTGTCGT	[7, 64]
X17	TGGATCAGAGTGGGAAGGGAGTCTTCAACTTGGCACCAAACCAACTTTAAGA	[7, 116]
X18	AGTTCGCGCTTGTTCATATCTTTTAACGCTGATCAGTCCCGATGGTTACTGT	[7, 38]
X19	GTAAGAAACGGAACCGCTGTAATTGCTCGGTGCACTTAAACCTAAGACCATT	[7, 90]
X20	CGTGAACGCGGTCACGCATACCGTTCGGCTGCTTAACTTACGCCAATATCAT	[9, 64]
X21	GCCATGGAAAAGGTAATGTACTGGTTACCACCGGTTGAAAGCTCCCGCATCC	[9, 116]
X22	TCACGCGATGATCCAGCGCTGAACCGGAGCACCAACTACAAACGTATTCCAA	[9, 38]
X23	GCGGATATACGGCGACCACCATGCCTTTCCCCATCCATATGTATTAACGATA	[9, 90]
X24	GCTGTTAATTTCCCATCAACCTTGCCCGGTGCAAAGCTATCTCTGCTGATAA	[11, 64]
X25	CATACAGCGCTTAGGGGTTGGTAGTGTGCGGGTTGGCTATGGCAACATAACG	[11, 116]
X26	GCTGACCGCGGACAACGTTCTGATTG	[11, 38]
X27	TATGAGGTCCTCGGGGACACATTACC	[11, 90]
X28	TCTTCTCCCGAATCGGAAGGGATTGG	[12, 39]
X29	TCGATCTCATGATTCTTTGGCAAATA	[12, 91]
X30	TAAAGCCTGCATTAAGTAATAATGCACTTACTTGTGGTACCTATCCACTAAT	[13, 38]
X31	GGCCCTTGTTTTCTTTATTAGTTCTGGTCTGGTCGCGCCTGGACAAAGGGAT	[13, 90]
X32	GCGAGGCCGCCGCGAGGTGCTAGGCTTCTACTTGTCCTAACCATAGGAACTA	[13, 64]

X33	GATGGCTATGGGAATCCGCCACGTACTGGTGATCATGAATCATGTCACGGTT	[13, 116]
X34	AGCTCCAGGTTCGGTGAACTTTGCGTAGGCGAACGGCTCAATTGGAACATCC	[15, 38]
X35	TAGCCTAGGACATTCTGATACCAACAACATTGCGAAGTTACATCTCTCGCTA	[15, 90]
X36	CCAATAGCCAGTTTTCAGTAGGCAGTCAGATGGAAGGAAAGTTGGCAGTATT	[15, 64]
X37	CGCTCGTTGACTGTCTTACTCTGGCTACCCCCGCAACAAAGAAGAGTTCCCG	[15, 116]
X38	GCTGGAGAAACTGAACCATGAACCGCCTCAGATACCAACATACAGCCGTGAG	[17, 38]
X39	ATAGAACGTAGCTCTCCGACCCCACCTGCCACATACGTTAGAGACAGTCCTT	[17, 90]
X40	GTTAAACTGAGCATTGCGGTTTTGAC	[17, 64]
X41	CTTCACTGCAGTTATATCTATCGACG	[17, 116]
X42	TTCATTAGGGGCGGAAATGGGCTGGT	[18, 13]
X43	TACCTGTGGGTAGGGCCGAGCGCTGG	[18, 65]
X44	TGCGAGCCCGTGAGGGTGCAAACGAAGCCCCACGTACAGTAACCAACCGGTG	[19, 64]
X45	ATTAATCATGACAATCGTGAACTCTGGCTTACATGTGAAAGGGAAATATATG	[19, 116]
X46	ATTCATGCTGAGTGCACCTTACGTGTTATGCGACACCATGATCCGGATGAGT	[19, 38]
X47	TTGTATCACCCATTTGGTATGGAGTCAGCTCGAAGTAAAACGTAGCACCCTT	[19, 90]
X48	AGCATCTGCACGGTGCGCTCACCCATTATGAAGATCGTCATTGGGATATAAA	[21, 64]
X49	GGGTCACTTTGGAGCAGGTTCAGTGAAGGAGATAGGGTAACCGCAGTAATAC	[21, 116]
X50	TCGATTATATGGTTCCTCCGGCCTCAGTTCCCTCTAGCTAGGGTGATGCCAA	[21, 38]
X51	TACATCTTGTCAGGAGCAAGCTGCTCTCTGATTTCTATTACCCTGGTATAAT	[21, 90]
X52	TTTGTATCCTGTGTTGTCAATTGGCAAAGGGTGGATATGGAGCTGGAACGGC	[23, 64]
X53	GATAGAAGAACTCTGATGGGCTCGCATGCGGCGCTACTTAGCCTCAATCATA	[23, 116]
X54	CTCATACTAACTCGGTGAATTGGACC	[23, 38]
X55	CGCAACTCAAGCATGGTAGGGATTCA	[23, 90]
Y00	CACTCAGCGGTCATTTTTTTTTTTTT	[0, 25]
Y01	GCTAGTAGGTCGTTTGAATTTTTCAC	[0, 77]
Y02	TTTTTTTTTTTTTGGGTGTTAGCCGT	[0, 129]
Y03	AGGAAAGTTCGCGAGAATCGCAAGGG	[1, 26]
Y04	CGGGATGCAGGCACCAATCGGCCCTA	[1, 78]
Y05	TCAAGACTCGGATTTTTTTTTTTTT	[2, 25]
Y06	TAGACCAATGCGAAATCGAGTATTCT	[2, 77]
Y07	TTTTTTTTTTTTTCCCCTTCGGGCGT	[2, 129]
Y08	GGGAATCGGACCGCCATTGTGCATCG	[3, 26]
Y09	CCTTTGATCGGGACCTTAACTGGGCC	[3, 78]
Y10	CCCTCAAATCTTTTTTTTTTTTTTT	[4, 25]
Y11	TTCAAGGGCTACTATGCTGAGGCAGC	[4, 77]
Y12	TTTTTTTTTTTTTGAAACCGGCCGCT	[4, 129]
Y13	ATTGCTTCTGGAAAGGATGACCAACT	[5, 26]
Y14	CGTTCGGACTGGGACTTATAGGAATT	[5, 78]

Y15	AATTCGTCCGCGGAGGCATTTGCACAGTCCGCGGTCAGCGGCAAGGTTGATG	[0, 51]
Y16	TAGGTAGCAATGAGTACCAGTCTATACGAGGACCTCATACACTACCAACCCC	[0, 103]
Y17	TACTCGTGCAGAAGTGAATACCGAGGGATCATCGCGTGAGAACGGTATGCGT	[2, 51]
Y18	TATATACCGTTGTTTTCTTTACGACTGCCGTATATCCGCAACCAGTACATTA	[2, 103]
Y19	GTCGTGCGACGGTAGACCCGCACATAACAAGCGCGAACTGTGCCAAGCGCAG	[4, 51]
Y20	AAGACTTCATCCTTTATAGCCCAGCTTTCCGTTTCTTACGAAGACTCCCTTC	[4, 103]
Y21	TCCCTAAGTATTGTTTTTTTTTTTTTTTTTTTTTTTTTTAACTGACACGTCT	[6, 25]
Y22	ATGGTTCCTGGCGACGACACCGCACGCCCTGAAGCGTTCGCGCACAAGCCCC	[6, 77]
Y23	TTTTTTTTTTTTTTCTTAAAGTTGGTGCCCAAGGCAGTATTTTTTTTTTTTT	[6, 129]
Y24	GGACTGATCAGCGTTTTTTTTTTTTTTTTTTTTTTTTTTTCTGCGACAGTTCC	[8, 25]
Y25	TTAAGTGCACCGAATGATATTGGCGTAAGCACGGGTAGAGATTACCGGATGA	[8, 77]
Y26	TTTTTTTTTTTTTGGATGCGGGAGCTCGGTCTGTGGCAGTTTTTTTTTTTTT	[8, 129]
Y27	GTAGTTGGTGCTCTTTTTTTTTTTTTTTTTTTTTTTTTTAATACGATTGATA	[10, 25]
Y28	TATGGATGGGGAATTATCAGCAGAGATCCTTCCCTCATAATCCAATAAGAGG	[10, 77]
Y29	TTTTTTTTTTTTTCGTTATGTTGCCACACTTGGCTTTCATTTTTTTTTTTTT	[10, 129]
Y30	TGCTCATAATCTGTTCTCGGATTCGCCAGTTTCTCCAGCGTCAAAACCGCAA	[6, 51]
Y31	TTGGTGCCAAGTTATTGGACCGCAATAGCTACGTTCTATCGTCGATAGATAT	[6, 103]
Y32	AAGTTAAGCAGCCACAGTAACCATCGCGAACCTGGAGCTACTGCCTACTGAA	[8, 51]
Y33	TTCAACCGGTGGTAATGGTCTTAGGTATGTCCTAGGCTAAGCCAGAGTAAGA	[8, 103]
Y34	TAGCTTTGCACCGTTGGAATACGTTTAATGCAGGCTTTAAGCCTAGCACCTC	[10, 51]
Y35	TAGCCAACCCGCATATCGTTAATACAGAAAACAAGGGCCGTACGTGGCGGAT	[10, 103]
Y36	TACCACAAGTAAGTTTTTTTTTTTTTTTTTTTTTTTTTTCAATCAGAACGTT	[12, 25]
Y37	GGCGCGACCAGACCCAATCCCTTCCGGGAAATTAACAGCGGTAATGTGTCCC	[12, 77]
Y38	TTTTTTTTTTTTTTATTTGCCAAAGATAAGCGCTGTATGTTTTTTTTTTTTT	[12, 129]
Y39	GAGCCGTTCGCCTTTTTTTTTTTTTTTTTTTTTTTTTTTCGGTTCAGCGCTG	[14, 25]
Y40	AACTTCGCAATGTTAGTTCCTATGGTGACCGCGTTCACGAGGCATGGTGGTC	[14, 77]
Y41	TTTTTTTTTTTTTAACCGTGACATGACCTTTTCCATGGCTTTTTTTTTTTTT	[14, 129]
Y42	GTTGGTATCTGAGTTTTTTTTTTTTTTTTTTTTTTTTTTTAAAAGATATGA	[16, 25]
Y43	AACGTATGTGGCAAATACTGCCAACTCTTGAACAAAACCGCAATTACAGCGG	[16, 77]
Y44	TTTTTTTTTTTTTCGGGAACTCTTCTCCACTCTGATCCATTTTTTTTTTTTT	[16, 129]
Y45	ATTCGGGAGAAGAATTAGTGGATAGGGAGTTAGTATGAGTGCCAATTGACAA	[12, 51]
Y46	ATCATGAGATCGAATCCCTTTGTCCATGCTTGAGTTGCGTGCGAGCCCATCA	[12, 103]
Y47	TAGGACAAGTAGAGGATGTTCCAATTACCATATAATCGAATGGGTGAGCGCA	[14, 51]
Y48	TTCATGATCACCATAGCGAGAGATGTCTGACAAGATGTATCACTGAACCTGC	[14, 103]
Y49	TTCCTTCCATCTGCTCACGGCTGTATACTCAGCATGAATTTCGTTTGCACCC	[16, 51]
Y50	TTGTTGCGGGGGTAAGGACTGTCTCTATGGGTGATACAACAGAGTTCACGAT	[16, 103]
Y51	CGCCCCTAATGAATTTTTTTTTTTTTTTTTTTTTTTTTTGCGGTTCATGGTT	[18, 25]
Y52	CTACCCACAGGTACACCGGTTGGTTATGCTCAGTTTAACGGTGGGGTCGGAG	[18, 77]

Y53	TTTTTTTTTTTTTCATATATTTCCCTAACTGCAGTGAAGTTTTTTTTTTTTT	[18, 129]
Y54	ATGGTGTCGCATATTTTTTTTTTTTTTTTTTTTTTTTTTTTACGCAAAGTTCAC	[20, 25]
Y55	TTTACTTCGAGCTTTTATATCCCAATAACTGGCTATTGGTGTTGGTATCAGA	[20, 77]
Y56	TTTTTTTTTTTTTGTATTACTGCGGTCAGTCAACGAGCGTTTTTTTTTTTTT	[20, 129]
Y57	AGCTAGAGGGAACTTTTTTTTTTTTTTTTTTTTTTTTTTTTTGCATTATTACTT	[22, 25]
Y58	AATAGAAATCAGAGCCGTTCCAGCTCGCGGCGGCCTCGCCAGAACTAATAAA	[22, 77]
Y59	TTTTTTTTTTTTTTATGATTGAGGCTTCCCATAGCCATCTTTTTTTTTTTTT	[22, 129]
Y60	CTGTACGTGGGGCACCAGCCCATTTC	[18, 51]
Y61	TTCACATGTAAGCCCAGCGCTCGGCC	[18, 103]
Y62	TTTTTTTTTTTTTACACGTAAGGTGC	[19, 0]
Y63	TCACGGGCTCGCAGACTCCATACCAA	[19, 52]
Y64	TGTCATGATTAATTTTTTTTTTTTTT	[19, 104]
Y65	GACGATCTTCATAACTCATCCGGATC	[20, 51]
Y66	TACCCTATCTCCTAAGGGTGCTACGT	[20, 103]
Y67	TTTTTTTTTTTTTTGAGGCCGGAGGA	[21, 0]
Y68	CCGTGCAGATGCTGAGCAGCTTGCTC	[21, 52]
Y69	TCCAAAGTGACCCTTTTTTTTTTTTT	[21, 104]
Y70	CATATCCACCCTTTTGGCATCACCCT	[22, 51]
Y71	AAGTAGCGCCGCAATTATACCAGGGT	[22, 103]
Y72	TTTTTTTTTTTTTGGTCCAATTCACC	[23, 0]
Y73	CACAGGATACAAATGAATCCCTACCA	[23, 52]
Y74	GAGTTCTTCTATCTTTTTTTTTTTTT	[23, 104]
X00	CCGCGGACGAATTGTGAAAAATTCA/3Alex647N/	
X03	TGCCTGCATCCCGCCTCTTATTGGATACGACCTACTAGCTATAGACTGGTA/3Cy3sp/	
X04	TATGAGGGAAGGACCCTTGCGATTCTTTCTGCACGAGTAAGAATACTCGAT/3Alex647N/	
X07	TCCCGATCAAAGGTCATCCGGTAATCTCGCATTGGTCTAAGTCGTAAAGAA/3Cy3sp/	
X08	TCTACCCGTGCTTCGATGCACAATGGACCGTCGCACGACGCTGCCTCAGCA/3Alex647N/	
X11	CCCAGTCCGAACGGGGGCTTGTGCGCAGTAGCCCTTGAAAGCTGGGCTATA/3Cy3sp/	
X15	CGCCAGGAACCATATTGCGGTCCAA/3Cy3sp/	
X16	GGTTTTGTTCAAGCTGCGCTTGGCACCAGATTATGAGCACGTGCGGTGTCG/3Alex647N/	
X19	GTAAGAAACGGAACCGCTGTAATTGCTCGGTGCACTTAAACCTAAGACCAT/3Cy3sp/	
X20	CGTGAACGCGGTCACGCATACCGTTCGGCTGCTTAACTTACGCCAATATCA/3Alex647N/	
X23	GCGGATATACGGCGACCACCATGCCTTTCCCCATCCATATGTATTAACGAT/3Cy3sp/	
X24	GCTGTTAATTTCCCATCAACCTTGCCCGGTGCAAAGCTATCTCTGCTGATA/3Alex647N/	
X28	TCTTCTCCCGAATCGGAAGGGATTG/3Alex647N/	
X31	GGCCCTTGTTTTCTTTATTAGTTCTGGTCTGGTCGCGCCTGGACAAAGGGA/3Cy3sp/	

X32	GCGAGGCCGCCGCGAGGTGCTAGGCTTCTACTTGTCCTAACCATAGGAACT/3Alex647N/	
X35	TAGCCTAGGACATTCTGATACCAACAACATTGCGAAGTTACATCTCTCGCT/3Cy3sp/	
X36	CCAATAGCCAGTTTTCAGTAGGCAGTCAGATGGAAGGAAAGTTGGCAGTAT/3Alex647N/	
X39	ATAGAACGTAGCTCTCCGACCCCACCTGCCACATACGTTAGAGACAGTCCT/3Cy3sp/	
X43	TACCTGTGGGTAGGGCCGAGCGCTG/3Cy3sp/	
X44	TGCGAGCCCGTGAGGGTGCAAACGAAGCCCCACGTACAGTAACCAACCGGT/3Alex647N/	
X47	TTGTATCACCCATTTGGTATGGAGTCAGCTCGAAGTAAAACGTAGCACCCT/3Cy3sp/	
X48	AGCATCTGCACGGTGCGCTCACCCATTATGAAGATCGTCATTGGGATATAAA[/3Alex647N/]	
X51	TACATCTTGTCAGGAGCAAGCTGCTCTCTGATTTCTATTACCCTGGTATAA/3Cy3sp/	
X52	TTTGTATCCTGTGTTGTCAATTGGCAAAGGGTGGATATGGAGCTGGAACGG/3Alex647N/	
Y01	/5Cy35/CTAGTAGGTCGTTTGAATTTTTCAC	
Y06	/5Cy35/AGACCAATGCGAAATCGAGTATTCT	
Y11	/5Cy35/TCAAGGGCTACTATGCTGAGGCAGC	
Y15	/5Cy55/ATTCGTCCGCGGAGGCATTTGCACAGTCCGCGGTCAGCGGCAAGGTTGATG	
Y16	/5Alex488N/AGGTAGCAATGAGTACCAGTCTATACGAGGACCTCATACACTACCAACCCC	
Y17	/5Cy55/ACTCGTGCAGAAGTGAATACCGAGGGATCATCGCGTGAGAACGGTATGCGT	
Y18	/5Alex488N/ATATACCGTTGTTTTCTTTACGACTGCCGTATATCCGCAACCAGTACATTA	
Y19	/5Cy55/TCGTGCGACGGTAGACCCGCACATAACAAGCGCGAACTGTGCCAAGCGCAG	
Y20	/5Alex488N/AGACTTCATCCTTTATAGCCCAGCTTTCCGTTTCTTACGAAGACTCCCTTC	
Y22	/5Cy35/TGGTTCCTGGCGACGACACCGCACGCCCTGAAGCGTTCGCGCACAAGCCCC	
Y25	/5Cy35/TAAGTGCACCGAATGATATTGGCGTAAGCACGGGTAGAGATTACCGGATGA	
Y28	/5Cy35/ATGGATGGGGAATTATCAGCAGAGATCCTTCCCTCATAATCCAATAAGAGG	
Y30	/5Cy55/GCTCATAATCTGTTCTCGGATTCGCCAGTTTCTCCAGCGTCAAAACCGCAA	
Y31	/5Alex488N/TGGTGCCAAGTTATTGGACCGCAATAGCTACGTTCTATCGTCGATAGATAT	
Y32	/5Cy55/AGTTAAGCAGCCACAGTAACCATCGCGAACCTGGAGCTACTGCCTACTGAA	
Y33	/5Alex488N/TCAACCGGTGGTAATGGTCTTAGGTATGTCCTAGGCTAAGCCAGAGTAAGA	
Y34	/5Cy55/AGCTTTGCACCGTTGGAATACGTTTAATGCAGGCTTTAAGCCTAGCACCTC	
Y35	/5Alex488N/AGCCAACCCGCATATCGTTAATACAGAAAACAAGGGCCGTACGTGGCGGAT	
Y37	/5Cy35/GCGCGACCAGACCCAATCCCTTCCGGGAAATTAACAGCGGTAATGTGTCCC	
Y40	/5Cy35/ACTTCGCAATGTTAGTTCCTATGGTGACCGCGTTCACGAGGCATGGTGGTC	
Y43	/5Cy35/ACGTATGTGGCAAATACTGCCAACTCTTGAACAAAACCGCAATTACAGCGG	
Y45	/5Cy55/TTCGGGAGAAGAATTAGTGGATAGGGAGTTAGTATGAGTGCCAATTGACAA	
Y46	/5Alex488N/TCATGAGATCGAATCCCTTTGTCCATGCTTGAGTTGCGTGCGAGCCCATCA	

Y47	/5Cy55/AGGACAAGTAGAGGATGTTCCAATTACCATATAATCGAATGGGTGAGCGCA	
Y48	/5Alex488N/TCATGATCACCATAGCGAGAGATGTCTGACAAGATGTATCACTGAACCTGC	
Y49	/5Cy55/TCCTTCCATCTGCTCACGGCTGTATACTCAGCATGAATTTCGTTTGCACCC	
Y50	/5Alex488N/TGTTGCGGGGGTAAGGACTGTCTCTATGGGTGATACAACAGAGTTCACGAT	
Y52	/5Cy35/TACCCACAGGTACACCGGTTGGTTATGCTCAGTTTAACGGTGGGGTCGGAG	
Y55	/5Cy35/TTACTTCGAGCTTTTATATCCCAATAACTGGCTATTGGTGTTGGTATCAGA	
Y58	/5Cy35/ATAGAAATCAGAGCCGTTCCAGCTCGCGGCGGCCTCGCCAGAACTAATAAA	
Y60	/5Cy55/TGTACGTGGGGCACCAGCCCATTTC	
Y61	/5Alex488N/TCACATGTAAGCCCAGCGCTCGGCC	
Y65	/5Cy55/ACGATCTTCATAACTCATCCGGATC	
Y66	/5Alex488N/ACCCTATCTCCTAAGGGTGCTACGT	
Y70	/5Cy55/ATATCCACCCTTTTGGCATCACCCT	
Y71	/5Alex488N/AGTAGCGCCGCAATTATACCAGGGT	

Dye-strands for various configurations

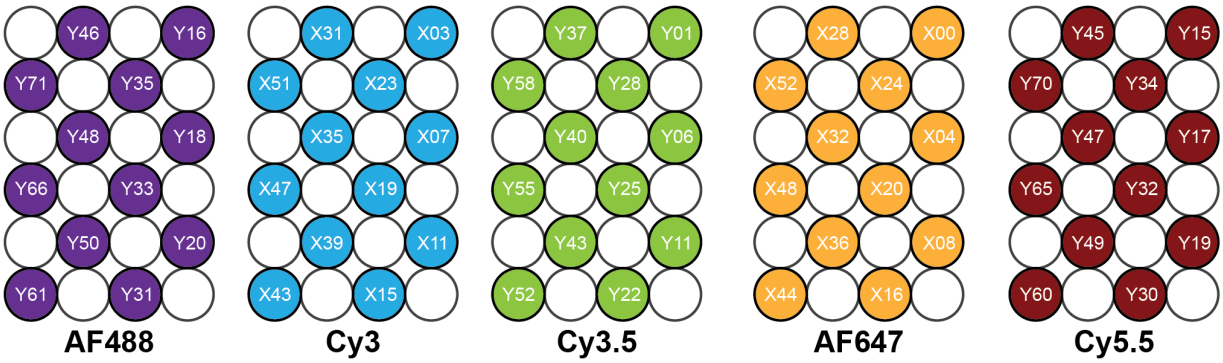

Figure S5: DNA strand cross-referencing index diagram for different dye positions. Each colored circle corresponds to the DNA strand replaced with the dye-modified analog for the various configurations tested. The DNA strands used in each configuration are represented in **Tables S2-S8** and each DNA strand name could be cross-referenced with the master DNA sequence **Table S1**.

Table S2: 1/1 configuration dye strands.

Dye	D1	D2	D3	D4	D5	D6	D7	D8	D9	D10	D11	D12
5'-AF488	Y33	Y48	Y50	Y35	Y66	Y18	Y20	Y71	Y31	Y46	Y61	Y16
3'-Cy3	X19	X35	X39	X23	X47	X07	X11	X51	X15	X31	X43	X03
5'-Cy3.5	Y25	Y40	Y43	Y28	Y55	Y06	Y11	Y58	Y22	Y37	Y52	Y01
3'-AF647	X20	X32	X36	X24	X48	X04	X08	X52	X16	X28	X44	X00
5'-Cy5.5	Y32	Y47	Y49	Y34	Y65	Y17	Y19	Y70	Y30	Y45	Y60	Y15

Table S3: 2/2 configuration dye strands.

Dye	D1	D2	D3	D4	D5	D6	D7	D8	D9	D10	D11	D12
5'-AF488	Y33	Y48	Y50	Y35	Y66	Y18	Y20	Y71	Y31	Y46	Y61	Y16
3'-Cy3	X19	X35	X39	X23	X47	X07	X11	X51	X15	X31	X43	X03
5'-Cy3.5	Y25	Y40	Y43	Y28	Y55	Y06	Y11	Y58	Y22	Y37	Y52	Y01
3'-AF647	X20	X32	X36	X24	X48	X04	X08	X52	X16	X28	X44	X00
5'-Cy5.5	Y32	Y47	Y49	Y34	Y65	Y17	Y19	Y70	Y30	Y45	Y60	Y15

Table S4: 3/3 configuration dye strands.

Dye	D1	D2	D3	D4	D5	D6	D7	D8	D9	D10	D11	D12
5'-AF488	Y33	Y48	Y50	Y35	Y66	Y18	Y20	Y71	Y31	Y46	Y61	Y16
3'-Cy3	X19	X35	X39	X23	X47	X07	X11	X51	X15	X31	X43	X03
5'-Cy3.5	Y25	Y40	Y43	Y28	Y55	Y06	Y11	Y58	Y22	Y37	Y52	Y01
3'-AF647	X20	X32	X36	X24	X48	X04	X08	X52	X16	X28	X44	X00
5'-Cy5.5	Y32	Y47	Y49	Y34	Y65	Y17	Y19	Y70	Y30	Y45	Y60	Y15

Table S5: 4/4 configuration dye strands.

Dye	D1	D2	D3	D4	D5	D6	D7	D8	D9	D10	D11	D12
5'-AF488	Y33	Y48	Y50	Y35	Y66	Y18	Y20	Y71	Y31	Y46	Y61	Y16
3'-Cy3	X19	X35	X39	X23	X47	X07	X11	X51	X15	X31	X43	X03
5'-Cy3.5	Y25	Y40	Y43	Y28	Y55	Y06	Y11	Y58	Y22	Y37	Y52	Y01
3'-AF647	X20	X32	X36	X24	X48	X04	X08	X52	X16	X28	X44	X00
5'-Cy5.5	Y32	Y47	Y49	Y34	Y65	Y17	Y19	Y70	Y30	Y45	Y60	Y15

Table S6: 8/8 configuration dye strands.

Dye	D1	D2	D3	D4	D5	D6	D7	D8	D9	D10	D11	D12
5'-AF488	Y33	Y48	Y50	Y35	Y66	Y18	Y20	Y71	Y31	Y46	Y61	Y16
3'-Cy3	X19	X35	X39	X23	X47	X07	X11	X51	X15	X31	X43	X03
5'-Cy3.5	Y25	Y40	Y43	Y28	Y55	Y06	Y11	Y58	Y22	Y37	Y52	Y01
3'-AF647	X20	X32	X36	X24	X48	X04	X08	X52	X16	X28	X44	X00
5'-Cy5.5	Y32	Y47	Y49	Y34	Y65	Y17	Y19	Y70	Y30	Y45	Y60	Y15

Table S7: 12/12 configuration dye strands.

Dye	D1	D2	D3	D4	D5	D6	D7	D8	D9	D10	D11	D12
5'-AF488	Y33	Y48	Y50	Y35	Y66	Y18	Y20	Y71	Y31	Y46	Y61	Y16
3'-Cy3	X19	X35	X39	X23	X47	X07	X11	X51	X15	X31	X43	X03
5'-Cy3.5	Y25	Y40	Y43	Y28	Y55	Y06	Y11	Y58	Y22	Y37	Y52	Y01
3'-AF647	X20	X32	X36	X24	X48	X04	X08	X52	X16	X28	X44	X00
5'-Cy5.5	Y32	Y47	Y49	Y34	Y65	Y17	Y19	Y70	Y30	Y45	Y60	Y15

Table S8: Pyramid configuration dye strands.

Dye	D1	D2	D3	D4	D5	D6	D7	D8	D9	D10	D11	D12
5'-AF488	Y33	Y48	Y50	Y35	Y66	Y18	Y20	Y71	Y31	Y46	Y61	Y16
3'-Cy3	X19	X35	X39	X23	X47	X07	X11	X51	X15	X31	X43	X03
5'-Cy3.5	Y25	Y40	Y43	Y28	Y55	Y06	Y11	Y58	Y22	Y37	Y52	Y01
3'-AF647	X20	X32	X36	X24	X48	X04	X08	X52	X16	X28	X44	X00
5'-Cy5.5	Y32	Y47	Y49	Y34	Y65	Y17	Y19	Y70	Y30	Y45	Y60	Y15

Spectroscopic Supplementary Data

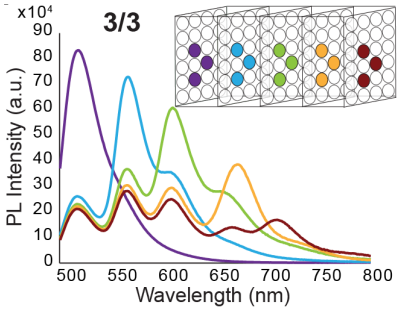

Figure S6: DNA blocks assembled with 3 copies of each dye per plane are, similar to Figure 3 (a-e).

Table S9: *Terminal Emission* of DNA Block structures as a function of the number of dyes per plane and the terminal acceptor dye. Data represented in Figure 3g main text.

	Terminal Acceptor			
DNA Block	**Cy3**	**Cy3.5**	**AF647**	**Cy5.5**
1/1	95.8 %	55.6 %	12.8 %	9.9 %
2/2	99.6 %	58.2 %	44.4 %	30.4 %
3/3	119.6 %	60.3 %	37.2 %	26.5 %
4/4	118.9 %	64.0 %	56.0 %	39.1 %
8/8	116.1 %	73.4 %	68.0 %	39.0 %
12/12	132.6 %	91.1 %	76.3 %	47.9 %
Pyramid	132.7 %	85.3 %	69.7 %	44.3 %

We estimate an uncertainty of ± 5% for all values. Values above 100% are due to increased absorption cross-section at the 466 nm wavelength used to excite the structures.

Table S10: FRET efficiency (E_{FRET}) of individual transfer from a D-plane to an A-plane as determined by steady-state fluorescence donor quenching of previous plane.

	Acceptor Dye			
DNA Block	**Cy3**	**Cy3.5**	**AF647**	**Cy5.5**
1/1	71 ± 5 %	56 ± 1 %	33 ± 12 %	82 ± 4 %
2/2	72 ± 4 %	60 ± 4 %	35 ± 5 %	79 ± 1 %
3/3	74 ± 2 %	49 ± 4 %	54 ± 4 %	83 ± 1 %
4/4	77 ± 2 %	65 ± 3 %	60 ± 3 %	63 ± 1 %
8/8	70 ± 2 %	72 ± 2 %	63 ± 1 %	84 ± 1 %
12/12	80 ± 2 %	83 ± 2 %	84 ± 2 %	89 ± 4 %
Pyramid	79 ± 2 %	75 ± 3 %	66 ± 4 %	76 ± 2 %

Antenna gain and anywhere-to-end efficiency section.

The ET characterization of DNA based photonic structures utilizes a few figures of merit including the End-to-End efficiency (E_{ee}) discussed in the main text. To provide additional insight and comparison to previously reported structures here we include Antenna Gain (AG) and Anywhere-to-End efficiency (E_{ae}) metrics.[1-4] In the current context, AG is a measure of the light-collection capability of the DNA block and is obtained experimentally by monitoring terminal Cy5.5 A emission (700 nm) integrated across the excitation wavelength range of 466-690 nm. AG predictions can be obtained using:

$$AG = \int_{\lambda_I}^{\lambda_F} \sum_d P(d_i, n) * E_{ee}(d_i, n) \times \sum_d [d_i] * \epsilon_{d_i}^{\lambda} \, d\lambda \qquad \text{(Eq. 1)}$$

where λ_I, and λ_F are the initial and final wavelengths, 466 and 690 nm, respectively, d represents the dye, i = (AF488, Cy3, Cy3.5, AF647, Cy5.5), and n is the number of dye copies per plane. $P(d_i,n)$ is the probability of exciting a particular dye as a function of the n where $[d_i]$ is the relative dye concentration and $\epsilon_{d_i}^{\lambda}$ is the extinction coefficient of the dye at the specific λ using:

$$P(d_i,n) = \frac{[d_i] * \epsilon_{d_i}^{\lambda}}{\sum [d_i] * \epsilon_{d_i}^{\lambda}} \qquad \text{(Eq. 2)}$$

The sum of the probability density function normalizes to 1 because we assume that every input photon is absorbed by one of the five dyes present in the DNA block. AG takes into consideration both the increase in light absorption due to the increased number of dyes as well as changes in E_{FRET} between dyes as their number and spatial distribution are changed. In short, AG is a measure of increased sensitization of the final A dye (Cy5.5) when the entire excitation spectra is taken into account.[3, 5] The AG values plotted in **Figure S7a** have been normalized to a DNA block with only a single Cy5.5 terminal A (0-0-0-0-1) present and, as shown, the greater the number of upstream dyes the greater the response. The effect is, however, not linear with the 1/1 assembly (5 dyes) only having an AG of 2.2 while the 12/12 assembly (60 dyes) displays a significantly increased AG of 48. Similar to the increased E_{ee} seen in **Figure 3h** of the main text, the non-linear increase of AG supports deviations from point-to-point transfer to point-to-plane as the number of dyes increased. To provide context for these values and this design, concentric or dendrimeric dye systems are typically used to optimize antenna effects such as AG. For example, using concentric dye placement on a DNA origami (13 dyes), Olejko and Bald obtained AG values of around 30,[6] while DNA dendrimers displaying 78 and 150 dyes achieved values of ~75 and ~150,

respectively.[1, 5] In contrast, using a hybrid DNA-phenanthrene light harvesting systems, the Häner group created large vesicular light harvesting systems (on the 100s of nm scale) capable of funneling light to a final DNA conjugated organic dye from which we extrapolated an *AG* value of ~15.[7-8] The current DNA block provides an intermediate position in both *AG* capability and overall structural size in comparison to these examples.

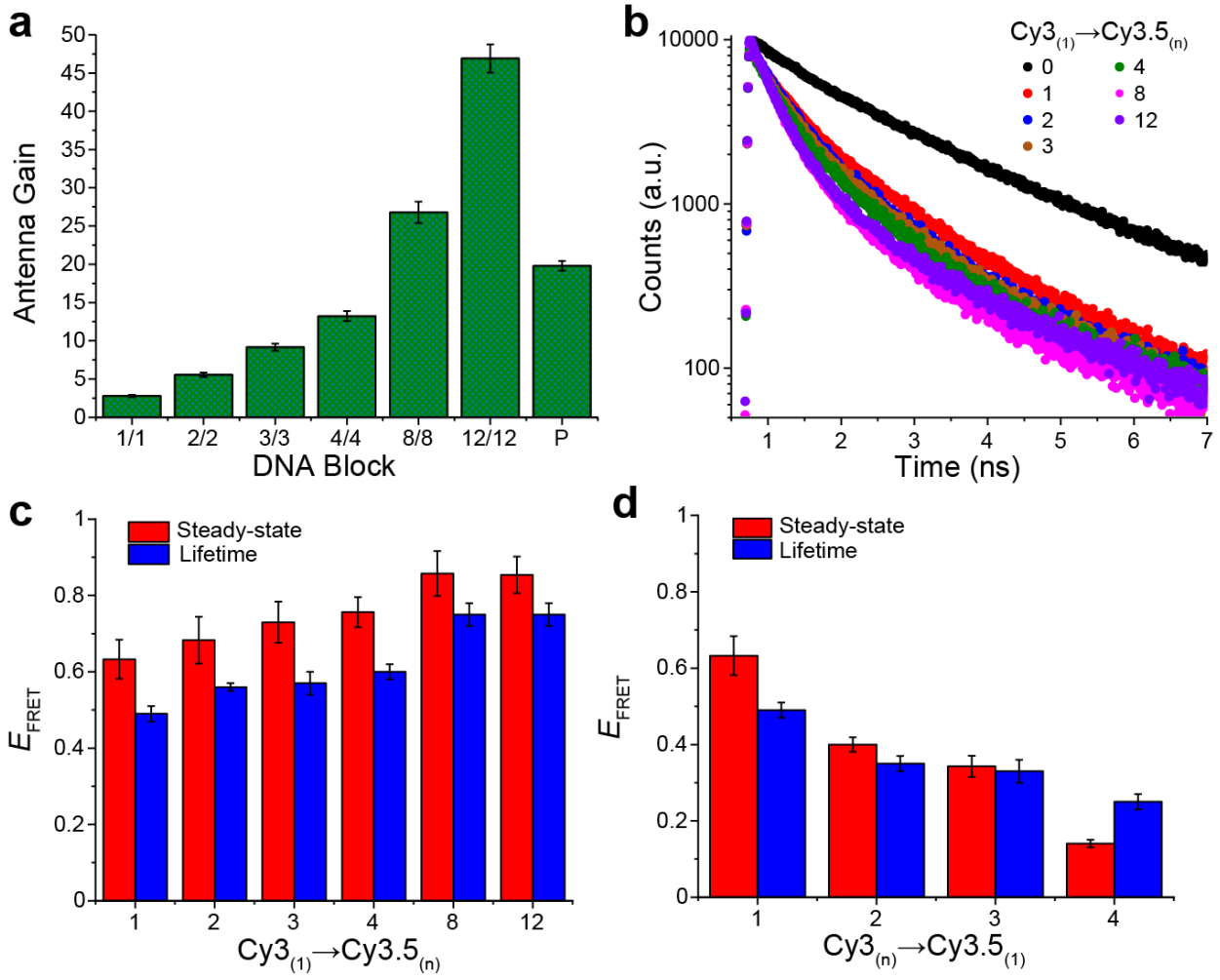

Figure S7: Antenna Gain and fluorescence lifetime measurements. (**a**) Antenna gain or AG values determined for the fully dye-labeled block configurations of Figure 3. Values are normalized to a DNA block with only a single Cy5.5 terminal A (0-0-0-0-1). **(b)** Representative example of fluorescence lifetimes collected from a single Cy3 D placed at the center of its plane as multiple Cy3.5 are built up on the adjacent A plane. Fits are based on double exponential decays. **(c)** FRET efficiency measured with steady-state fluorescence or TCSPC-based excited-state lifetimes from a single central Cy3 D to multiple Cy3.5 A's placed in the adjacent plane. **(d)** FRET efficiency measured with steady-state fluorescence or TCSPC-based excited-state lifetimes from a plane of donors composed of 1, 2, 3, or 4-Cy3 D dyes to a single Cy3.5 A located on position H8/D1 (referring to **Figure S1** positioning).

Steady state and TCSPC fluorescence lifetime FRET values are presented for Cy3 D→Cy3.5 A pair while varying A ratios (**Figure S7c**). The general trend of the two methodologies was consistent, though for final analysis lifetimes were employed since these provide a more precise measurement with its limited sensitivity to concentration and inner filter effects; not that this was expected to be an issue at the low concentrations of samples utilized throughout. Complimentary to **Figure S7c**, experiments which placed a single Cy3.5 A in the D1 position and increased the number of Cy3 D's from one to four were realized. Since the E_{FRET} of Cy3 D dyes in the 2, 3, and 4 positions to the Cy3.5 A is predicted to be less than that of D1, it would be expected that overall E_{FRET} decreases, these results can be found in **Figure S7d**.

E_{ae} resembles E_{ee} but is sensitive to and accounts for absorption by downstream dyes beyond the initial D molecules. E_{ae} is defined almost the same as Eq. 1 but with a corrective factor and is experimentally simpler to determine and can provide insight into increased antenna properties, but is typically only useful for comparisons of systems where the number and ratio of dyes is unchanged.

$$E_{ae} = 100 * {[(\Phi_{AD} - \Phi_A)/Q_A]}/{(\Phi_D/Q_D)} \qquad \text{(Eq. S3)}$$

Φ_{AD} and Φ_A are the A emission (Cy5.5 dye) in the presence of D or the A alone, respectively, Φ_D is the emission of the D (AF488) only, while Q_A and Q_D are the quantum yields of the AF488 D and Cy5.5 A. Particular values and analysis of E_{ae} is available in **Section VI** of the **SI**.

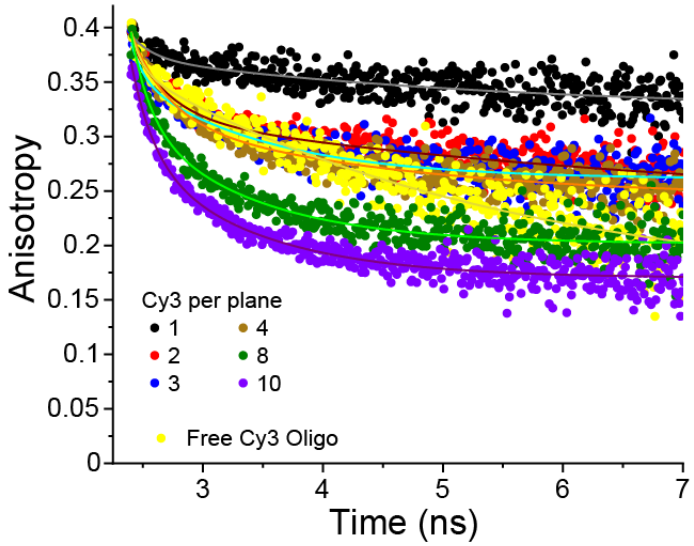

Figure S8: Fluorescence lifetime anisotropy reflecting intra-plane homoFRET from block assemblies where Cy3 dye density was increased. The yellow curve represents a Cy3-labeled brick alone without the entire DNA block assembled around it. Fits are to double exponential decays.

Table S11: Fluorescence lifetime anisotropy fitting parameters. Data from **Figure S8**.

Sample	y_0	A_1	τ_1	A_2	τ_2	$\langle\tau\rangle$
1 Cy3 Block	0.32 ± 0.01	0.02 ± 0.01	0.19 ± 0.01	0.05 ± 0.01	5.04 ± 0.38	3.6 ± 0.7
2 Cy3 Block	0.23 ± 0.04	0.05 ± 0.01	0.32 ± 0.06	0.09 ± 0.02	3.12 ± 0.16	2.1 ± 0.4
3 Cy3 Block	0.26 ± 0.01	0.03 ± 0.01	0.11 ± 0.03	0.09 ± 0.02	1.12 ± 0.12	0.9 ± 0.2
4 Cy3 Block	0.24 ± 0.01	0.07 ± 0.01	0.30 ± 0.06	0.07 ± 0.02	2.09 ± 0.26	1.2 ± 0.3
8 Cy3 Block	0.20 ± 0.01	0.11 ± 0.02	0.98 ± 0.13	0.09 ± 0.02	0.16 ± 0.06	0.6 ± 0.1
10 Cy3 Block	0.18 ± 0.01	0.10 ± 0.02	1.01 ± 0.12	0.04 ± 0.01	0.19 ± 0.05	0.8 ± 0.2
Free Cy3 Oligo	0.16 ± 0.01	0.006 ± 0.001	0.09 ± 0.03	0.19 ± 0.01	3.11 ± 0.40	3.0 ± 0.5

Fit: $y(t) = y_0 + a_1 e^{-t/\tau_1} + a_2 e^{-t/\tau_2}$. $\langle\tau\rangle = ((A_1 * \tau_1) + (A_2 * \tau_2))/(A_1 * A_2)$

Simulation of Ideal Sheet Behavior FRET

For the calculations discussed in the main text in the *'Simulations of ideal sheet behavior with discrete dyes'* section and **Figure 4** of the main text, we continue to use the Förster transfer rate in Eq. (3) and model the evolution of the excitation probabilities of each dye using rate equations that include all possible FRET processes, as well as any radiative (or potentially non-radiative) channels.[4] For computing the transfer efficiency, we need to know only the total acceptor emission (per photon absorbed by the donor), and the problem thereby reduces to a linear algebra obtained by integrating the rate equations over time.[4]

Manuscript Figure 4 focuses on the behavior of dye arrays in the dynamic dipole limit. However, fluorescence anisotropy measurements on the DNA arrays provide strong evidence that the dipoles are closer to being static on the time scale of the fluorescence decay. Thus, it is worth examining how the behavior changes when we switch from an assumption of dynamic dipoles to the static limit. **Figure S10a**, **d** shows simulation results assuming fully random-static dipoles. For any given r value the efficiency for the static dipole case is always less than that for the dynamic case. The crossing of the curves seen here occurs because the ensemble average of R_0 in the static case turns out to be about 5.7 nm as compared to the 6.4 of the dynamic limit, and so shifts the static curve uniformly to the left. As is evident from the plot, the limits with exponents of either 4 or 6 are no longer realized, and instead the slopes vary continuously in all cases, gradually increasing from ~3 to ~5 over the range of c/R_0 studied. This suggests that no matter what the dimensions of an experimental array are, a clean signature of a sheet-regime slope of 4 may not be seen. Nevertheless, as **Figure S10d** also shows, we can still expect a significant increase in R_{0eff} if we are able to access a dimensional regime where a/c is less than 1.

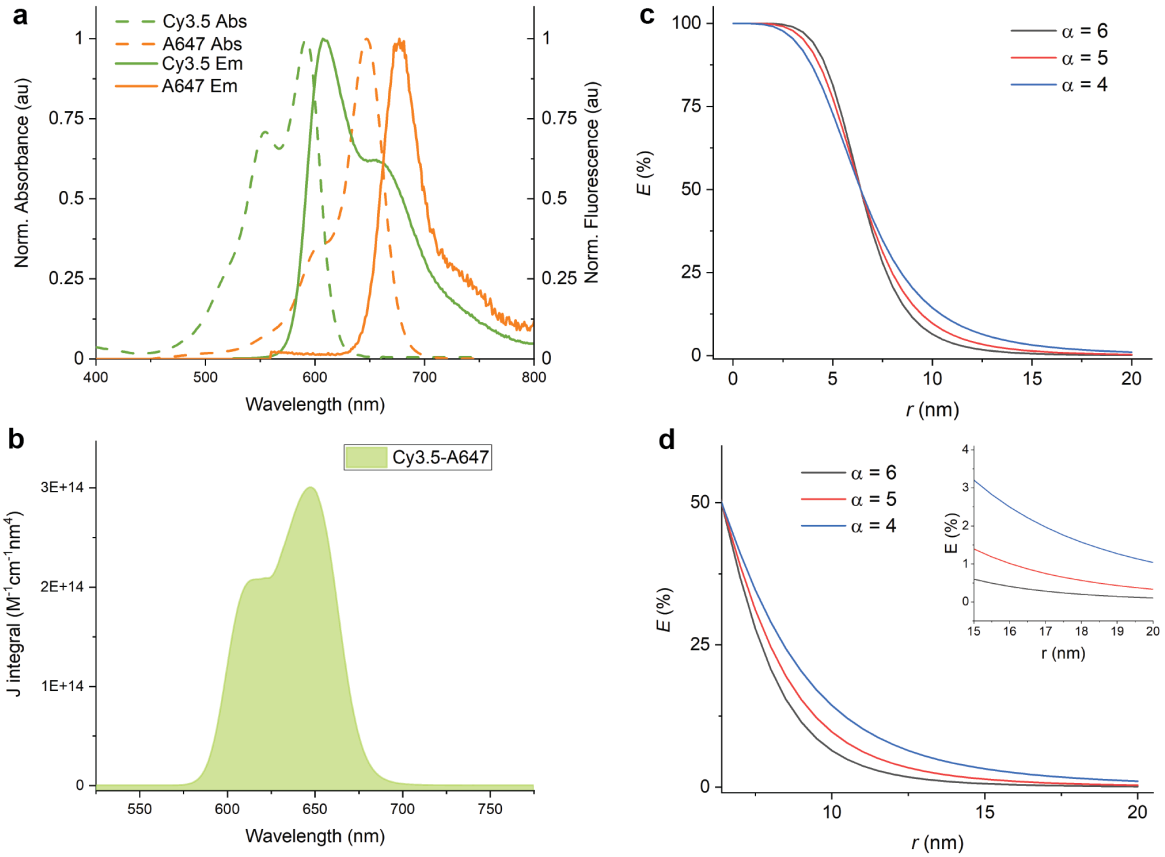

Figure S9: Spectral properties of Cy3.5 (donor) -A647 (acceptor) point-to-point pair. (a) Normalized absorbance and emission profiles. **(b)** Spectral overlap integral between Cy3.5 and A647. **(c, d)** Point to point FRET efficiency *versus* dye separation as a function of different exponent α values of 4, 5, 6.

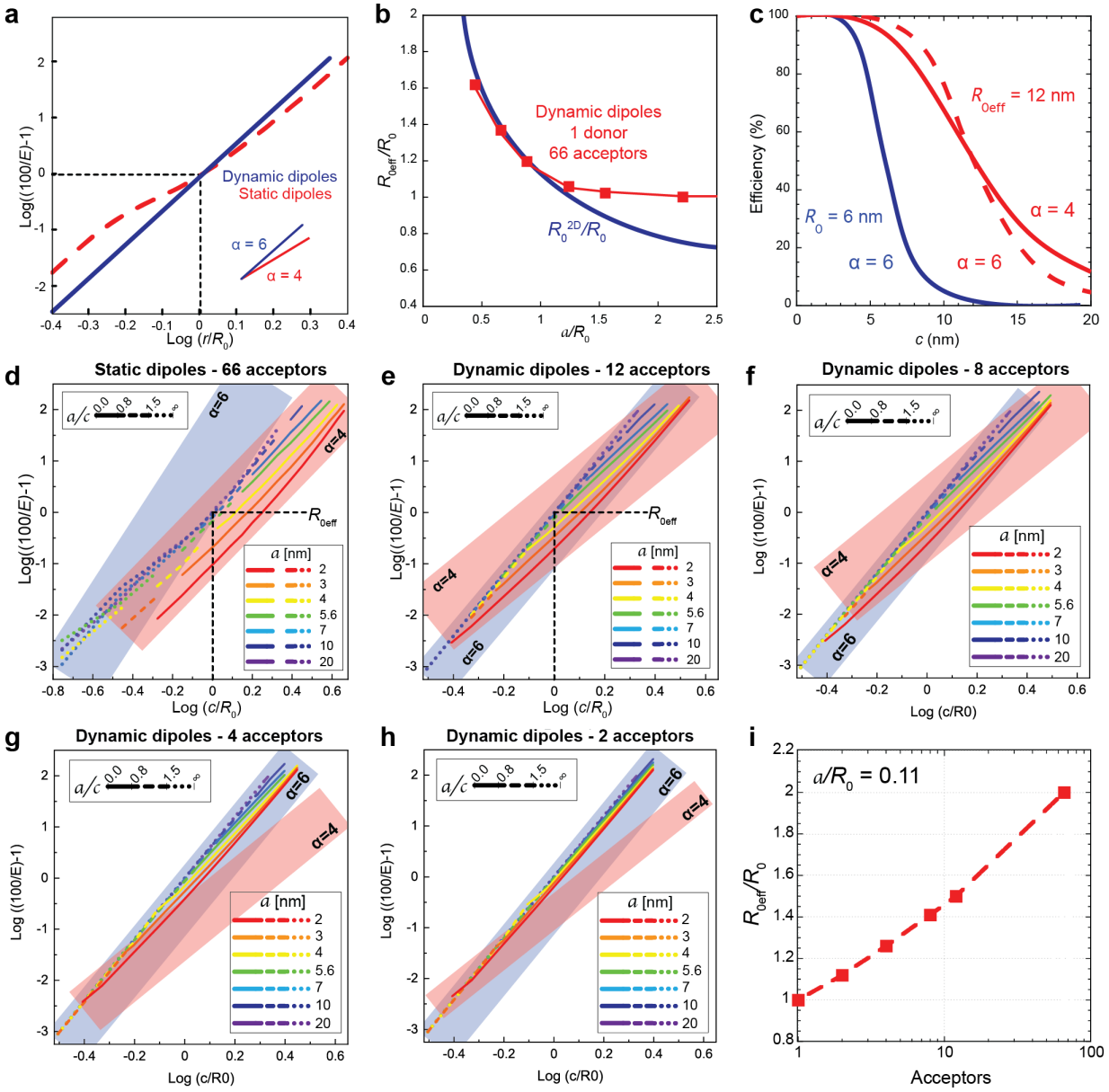

Figure S10: FRET simulations for a single donor with a sheet of acceptors. (a) Log-log plot of scaled FRET efficiency (E_{FRET}) for a single D-A pair *versus* the scaled D-A distance assuming dynamic or static dipoles**.** The slope assuming static dipoles is no longer fixed at 6, but can be less especially in the vicinity of r = R_0. **(b)** Effective R_0 (R_{0eff}) as derived from Fig 4(b) *versus a* (with both normalized by R_0) and compared with the sheet approximation. (**c**) The efficiency versus *c* showing the increased range in the ideal dye-sheet regime and showing that the R_{0eff} value is usually more important in determining the range. **(d)** Log-log plot of E_{FRET} with the Cy3.5 and AF647 as the D-A sheet pair *versus* c/R_0 assuming a static dipole configuration. Values of *a* are treated the same as in (b). **(e)** Log-log plot of E_{FRET} with a D-A sheet consisting of a single Cy3.5 D and 12-AF647 A's *versus* c/R_0 assuming a dynamic dipole configuration. Values of *a* are treated the same as in Fig 4(b). Analogous to Figure 4b with **(f)** 8, **(g)** 4, and **(h)** 2 acceptors included in the sheet. The plots show that with fewer acceptors present the edge-dominated right limit of the characteristic curves moves leftward and results in a decreasing range of possible R_{0eff} values as is also illustrated in (i) for a particular (small) value of a/R_0.

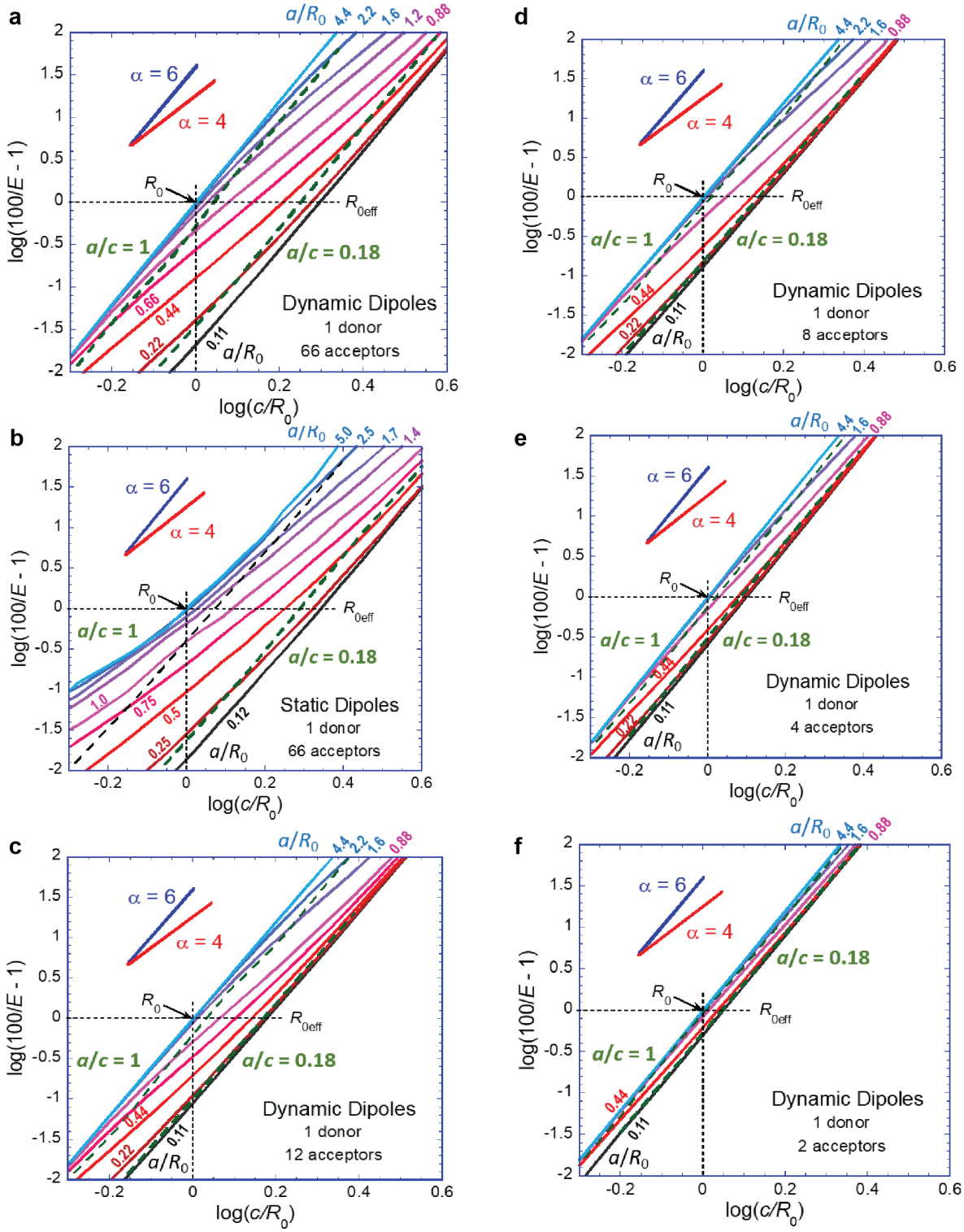

Figure S11: Alternative representations of Figure **S10 (a-c)** plotting log(100/*E*-1) *versus* log(c/R_0) with a/R_0 as a parameter assuming 1 donor, 66 acceptors, and either **(a)** dynamic dipoles or **(b)** static dipoles. Identical to **(a)** except having different number of acceptors are shown in **(c)** 12 acceptors, **(d)** 8, **(e)** 4, and **(f)** 2 acceptors.

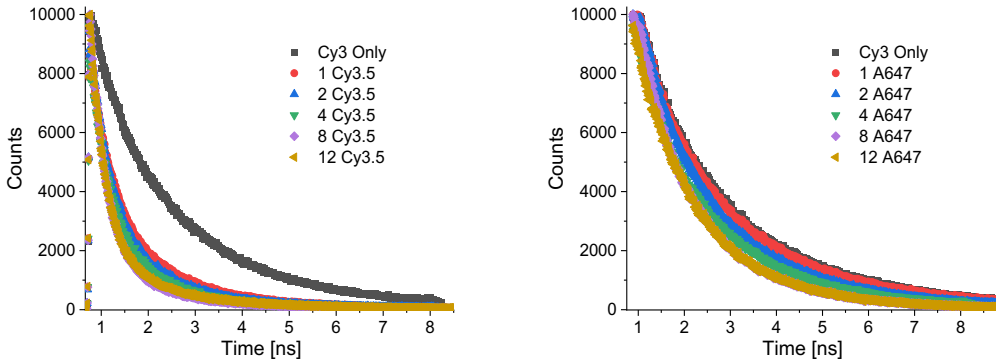

Figure S12: Fluorescence lifetime of $Cy3_{(1)} \rightarrow Cy3.5_{(n)}$ and $AF647_{(n)}$. The excitation laser was a 80 MHz 7 ps pulsed 532 nm frequency-doubled diode-pumped Nd:YVO4 laser (High-Q picoTRAIN), detection was at 565 nm. *Left:* Cy3.5 acceptors. *Right:* A647 acceptors.

Table S12: Amplitude averaged fluorescence lifetime of Cy3 in $Cy3_{(1)} \rightarrow Cy3.5_{(n)}$ and $AF647_{(n)}$. The excitation laser was a 80 MHz 7 ps pulsed 532 nm frequency-doubled diode-pumped Nd:YVO4 laser (High-Q picoTRAIN), detection was at 565 nm.

Sample	A_1	τ_1	A_2	τ_2	lifetime $\langle\tau\rangle$
Cy3 alone	7811	0.81	10213	1.87	1.61 ± 0.01 ns
Cy3.5 Acceptor					
1 Acceptor	29718	0.49	5774	1.42	0.827 ± 0.005 ns
2 Acceptors	35052	0.44	4276	1.41	0.711 ± 0.004 ns
4 Acceptors	38788	0.41	3941	1.35	0.643 ± 0.004 ns
8 Acceptors	84314	0.31	1989	1.30	0.400 ± 0.005 ns
12 Acceptors	78821	0.30	2080	1.31	0.410 ± 0.005 ns
A647 Acceptor					
1 Acceptor	2029	0.80	8437	1.60	1.51 ± 0.01 ns
2 Acceptors	2365	0.62	7489	1.56	1.46 ± 0.01 ns
4 Acceptors	5032	0.42	4517	1.52	1.26 ± 0.01 ns
8 Acceptors	6042	0.38	3149	1.49	1.13 ± 0.01 ns
12 Acceptors	6975	0.33	2963	1.44	1.05 ± 0.01 ns

Note: R-Squared of fit in all cases > 0.99.

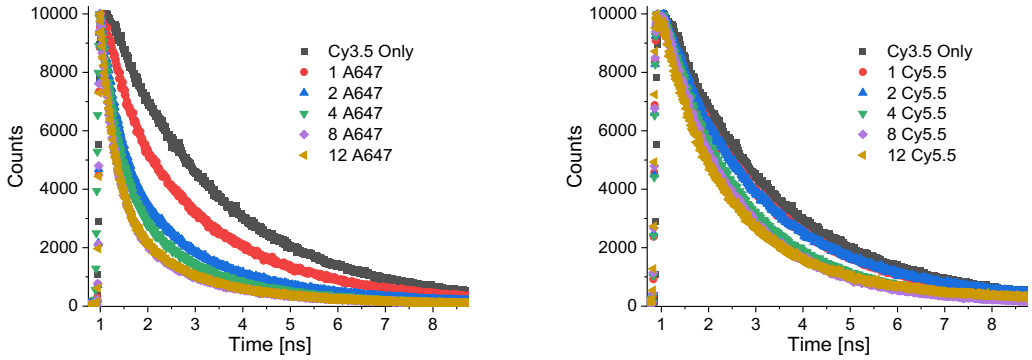

Figure S13: Fluorescence lifetime of Cy3.5$_{(1)}$ → AF647$_{(n)}$ and Cy5.5$_{(n)}$ with varying number of acceptors. The excitation laser was a 80 MHz 7 ps pulsed 532 nm frequency-doubled diode-pumped Nd:YVO4 laser (High-Q picoTRAIN), detection was at 620 nm. *Left:* A647 acceptors. *Right:* Cy5.5 acceptors.

Table S13: Amplitude averaged fluorescence lifetime of Cy3.5 in Cy3.5$_{(1)}$ → AF647$_{(n)}$ and Cy5.5$_{(n)}$. The excitation laser was a 80 MHz 7 ps pulsed 532 nm frequency-doubled diode-pumped Nd:YVO4 laser (High-Q picoTRAIN), detection was at 620 nm.

Sample	A_1	τ_1	A_2	τ_2	lifetime $\langle\tau\rangle$
Cy3.5 alone	2593	1.60	5278	2.46	2.25 ± 0.01 ns
A647 Acceptor					
1 Acceptor	8893	0.58	2056	2.26	1.37 ± 0.01 ns
2 Acceptors	8502	0.42	1898	1.90	1.17 ± 0.01 ns
4 Acceptors	9900	0.41	879	1.79	0.79 ± 0.01 ns
8 Acceptors	11157	0.34	504	1.65	0.57 ± 0.01 ns
12 Acceptors	10838	0.34	491	1.59	0.56 ± 0.01 ns
Cy5.5 Acceptor					
1 Acceptor	1286	0.96	9356	2.31	2.05 ± 0.01 ns
2 Acceptors	9677	1.76	7441	2.16	1.96 ± 0.01 ns
4 Acceptors	8629	1.28	6571	2.13	1.64 ± 0.01 ns
8 Acceptors	6278	1.01	4710	2.04	1.46 ± 0.01 ns
12 Acceptors	4784	0.79	4844	1.90	1.35 ± 0.01 ns

Note: R-Squared of fit in all cases > 0.99.

Table S14: Energy transfer efficiency of $D_{(1)} \rightarrow A_{(n)}$ systems. Values for data in **Figure 5**.

Dye-Pairs		Cy3→Cy3.5	Cy3→A647	Cy3.5→A647	Cy3.5→Cy5.5
1 Acceptor	Experimental	0.49 ± 0.02	0.052 ± 0.005	0.39 ± 0.04	0.09 ± 0.03
	Predicted	0.50	0.05	0.39	0.09
2 Acceptors	Experimental	0.56 ± 0.01	0.090 ± 0.005	0.48 ± 0.03	0.13 ± 0.04
	Predicted	0.57	0.08	0.46	0.13
4 Acceptors	Experimental	0.60 ± 0.02	0.22 ± 0.02	0.65 ± 0.02	0.27 ± 0.02
	Predicted	0.59	0.16	0.55	0.25
8 Acceptors	Experimental	0.75 ± 0.03	0.30 ± 0.02	0.75 ± 0.03	0.35 ± 0.02
	Predicted	0.74	0.30	0.67	0.40
12 Acceptors	Experimental	0.75 ± 0.03	0.34 ± 0.02	0.75 ± 0.04	0.40 ± 0.02
	Predicted	0.76	0.38	0.70	0.47

The $Cy3_{(1)} \rightarrow Cy3.5_{(3)}$ system was measured as 0.57 ± 0.03 and the predicted value was 0.59.

MD Simulations and FRET Predictions

Molecular dynamics simulation of the DNA Block

To obtain more information about the DNA block we performed atomistic molecular dynamics (MD) simulations in which the DNA nanostructure plus its attached dyes, surrounding water molecules, and counter-ions are evolved according to the laws of classical mechanics with prescribed force fields that parameterize the various interactions. When run long enough, such simulations fully explore the phase space of any given structure, and in this way allow for a complete characterization of its equilibrium and its fluctuations to the extent that the assumed force fields are accurate.

The molecular model for the DNA block was generated using CaDNAno[9] and NanoHub[10-11] to which the dyes were added using Chimera (UCSF, CA).[12] The MD was then performed using the Gromacs 5.1.5 package[13] with Amber99sb force field parameters for the DNA[14], the generalized Amber force field (GAFF) for the dyes[15], and with the structure solvated using the TIP3P water model[16] with a 20 mM $MgCl_2$ buffer. All other aspects (boundary conditions, energy minimization, pressure, temperature conditions, *etc*.) were the same as reported previously.[17] The time step used was 2 fsec, and the total time simulated was 1 μsec. Whether the latter is long enough to fully capture the slow modes that the large structure can support and the slow fluctuations of the dyes in the DNA energy landscape (and especially of AF647 with its long linker) is not known.

Because of the large size of the block (see **Figure 1** and **Figure 6a**), the job of simulating the DNA block using MD is computationally very intensive, and especially so given the number of different dye arrangements that were considered. To reduce the computational burden, we therefore introduced several simplifications.

1. We mildly constrained (with weak harmonic springs attached to a few P atoms) the DNA block so as to prevent it from rotating, and thereby allowing the size of the box in which the MD simulation is carried out to be greatly reduced. The P atoms constrained in this manner were at the edges of the DNA block, relatively far from the dyes so as to not expect the constrains to affect the dye dynamics. Even so, the full block plus its surrounding water and counterions involved around 900,000 atoms and simulating the 1 μsec transient required roughly one month on our cluster.

2. We performed just a single MD simulation of the full block with one copy of each different dye assembled along its center line (specifically on H8 in **Figure S1b** which hosts D1 as shown in **Figure S1c**), and then approximated all other dye configurations based on this simulation. To this end, we note that the MD simulation provides time histories for the attachment points of all possible dyes. In addition, it gives histories of the relative position of each D1 dye on H8 with respect to its local DNA. We then assumed that this same relative motion occurred for the other possible dyes (away from H8), just rotated so as to match the local orientation of the DNA duplex to which it is attached. In this way, we obtained approximations for the positions of any dye within the DNA block, and this information was then used as the input to our MD-based FRET simulations as explained below. The main source of error in this approach is that we are ignoring the perturbing effect the non-H8/D1 dyes have on the DNA block motion (which again is taken to be that obtained with only the H8/D1 dyes present).

MD-derived distance and orientation distributions for 1 donor and multiple acceptors

The ideal simulations assume the dye positions are prescribed and that the dipole orientations are uniformly random (whether dynamic or static). To test these assumptions, we employed MD simulations. Using MD results to predict FRET is easy if the dye motions can be treated as static, and this is assumed in this paper. Under this assumption, the approach is again to use a Monte Carlo algorithm, but now the dye positions are no longer assumed known and the orientations no longer uniformly random, but instead they are obtained by sampling the MD histories (with the initial transient ignored) for each instantiation in the FRET simulation. In doing this, each FRET calculation would in principle use the positions and orientations for all dyes at the *same* random time in the MD simulation in order to preserve correlations. However, our treatment of the non-H8/D1 dyes gives all dyes of the same type the same relative motion with respect to the DNA, and this would seem to introduce spurious correlations if all dye positions/orientations were taken at the same random time. Therefore, for non-H8/D1 dyes we take their attachment points to be at the same random time but the relative motions of each of those dyes with respect to their attachment points are instead selected from a *different* random time. Then as before, after analyzing many such instantiations, the ensemble of FRET simulation results is averaged to obtain the FRET efficiencies. One other non-ideality sometimes included in these simulations is a representation of

the fact that the dyes need not all be present and active in real experiments. Our approach in this regard is simply to give each dye a known (and high) probability of being present in any given instantiation of the Monte Carlo procedure. The broad results are available in **Table 3** and **Figure 6** of the main text with detailed results presented in **Figures S14-S17.**

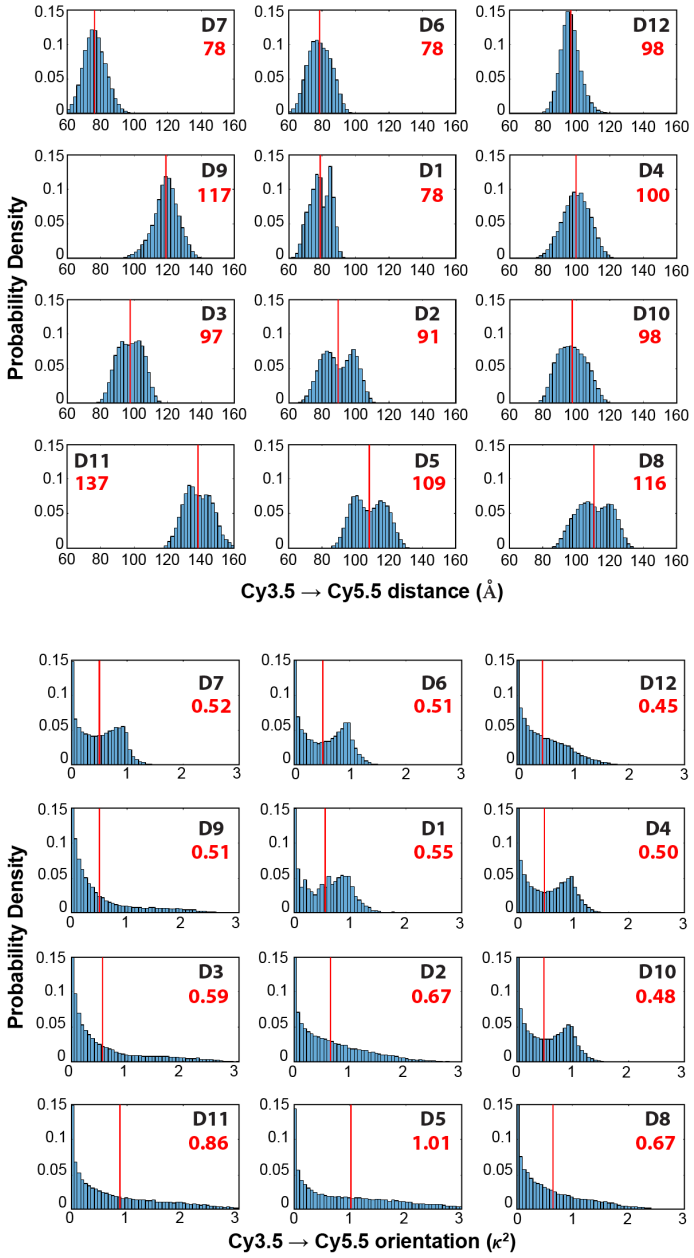

Figure S14: Probability density of Cy3.5$_{(1)}$ → Cy5.5$_{(1\text{-}12)}$ spacing and dipole orientation. The labeling corresponds to that of **Figure S1**. Numbers in red indicate approximate mean values (shown as vertical red lines).

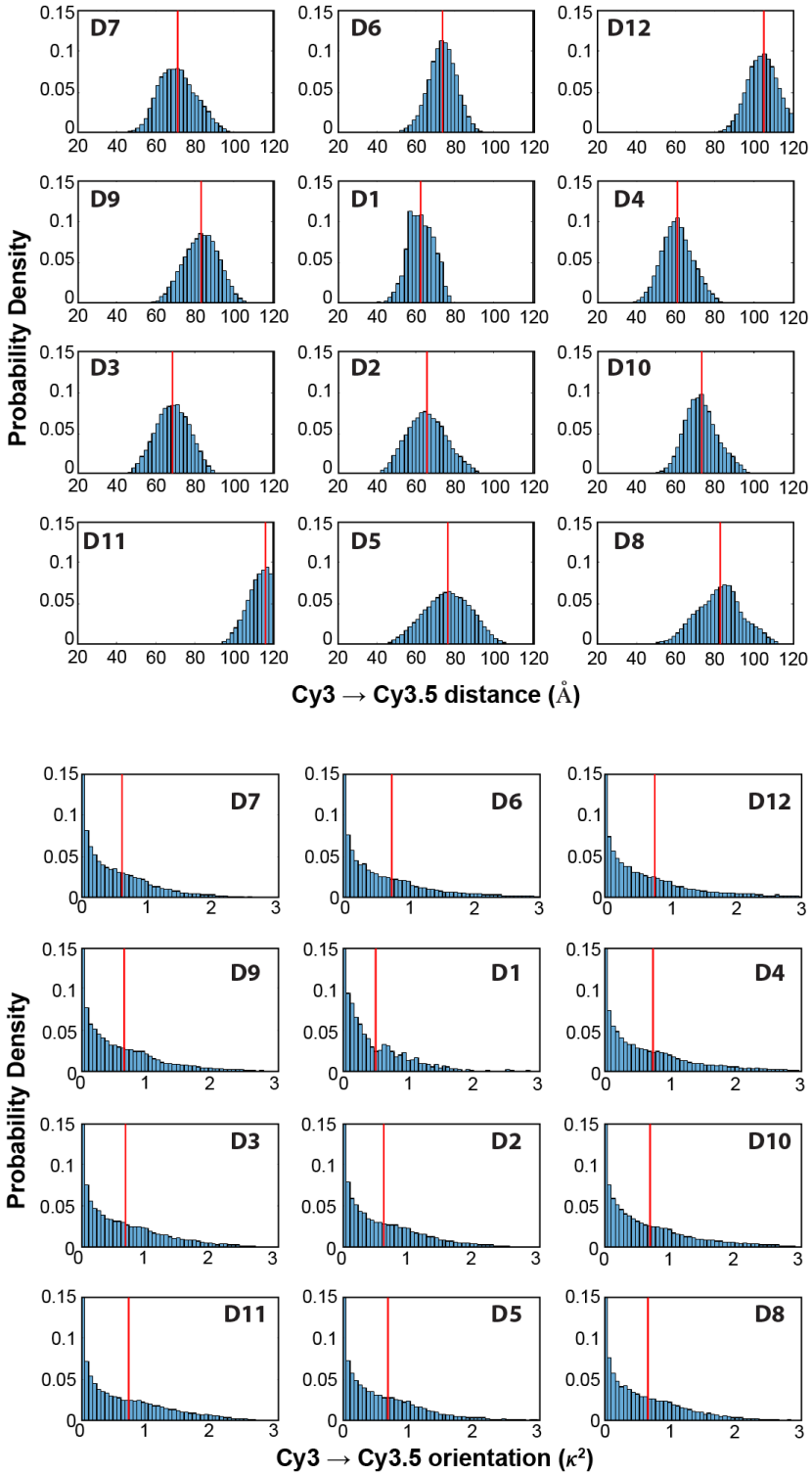

Figure S15: Probability density of $Cy3_{(1)}$ → $Cy3.5_{(1\text{-}12)}$ spacing and dipole orientation. The labeling corresponds to that of **Figure S1**.

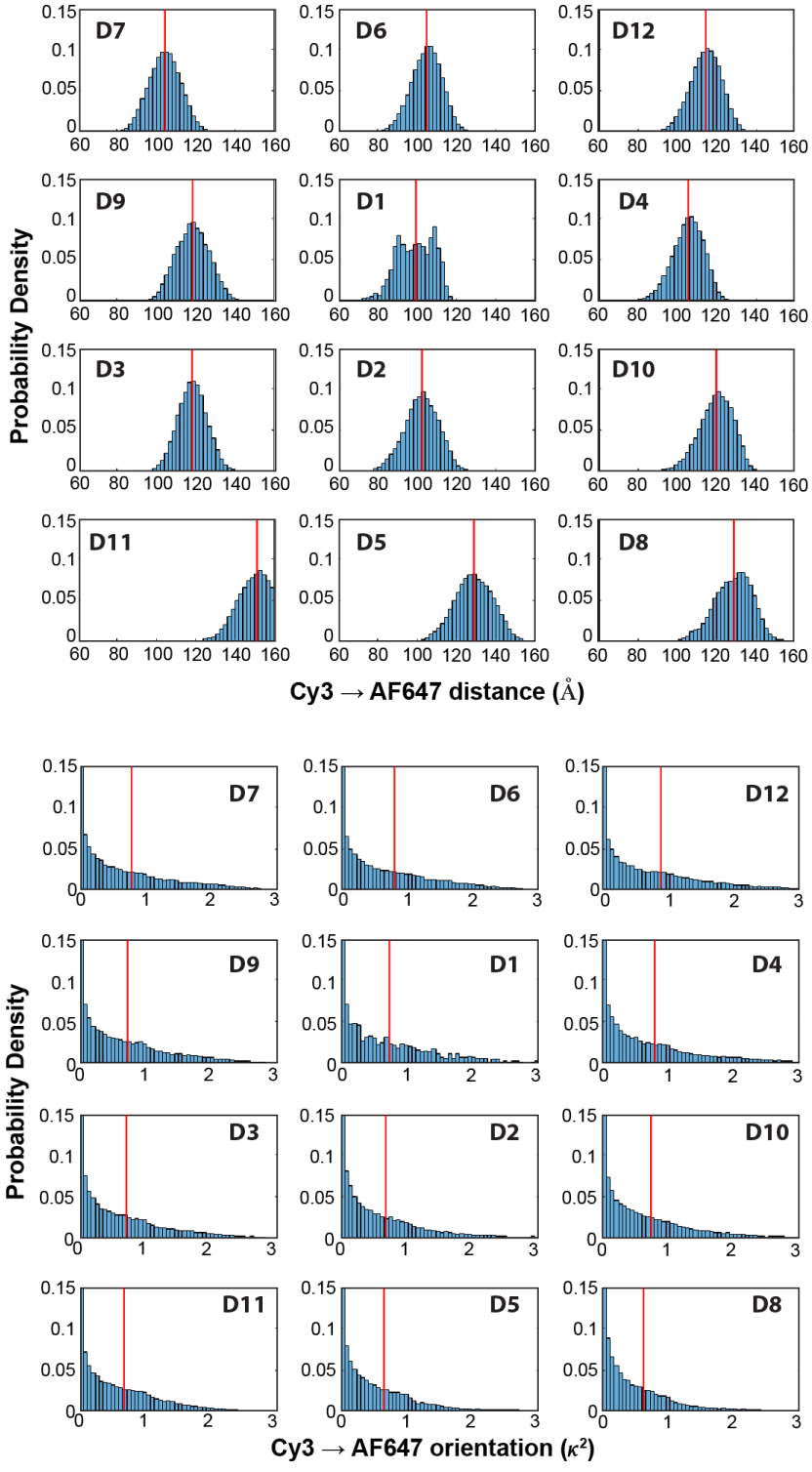

Figure S16: Probability density of distributions of $Cy3_{(1)}$ →$AF647_{(1\text{-}12)}$ and dipole orientation. The labeling corresponds to that of **Figure S1**.

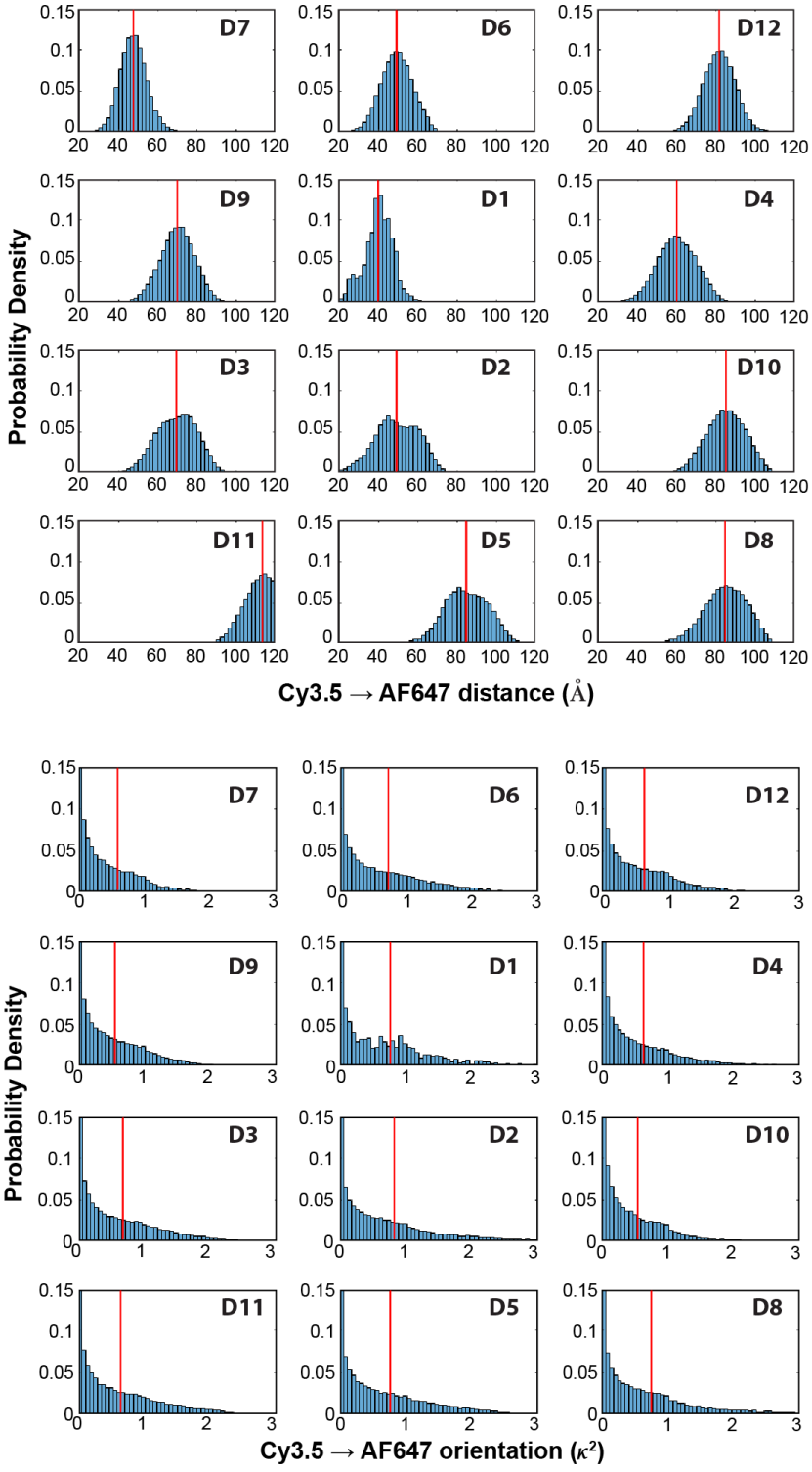

Figure S17: Probability density of distribution of Cy3.5$_{(1)}$ → AF647$_{(1-12)}$ and dipole orientation. The labeling corresponds to that of **Figure S1**.

Experimental Efficiencies vs. MD-based FRET Simulations

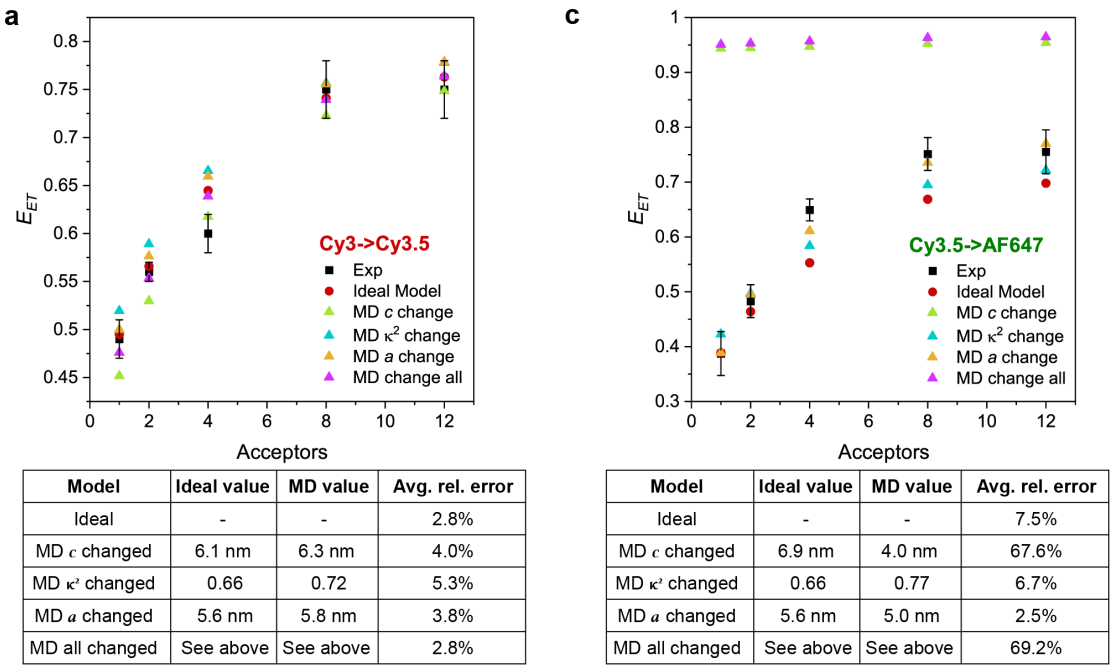

Model	Ideal value	MD value	Avg. rel. error
Ideal	-	-	2.8%
MD c changed	6.1 nm	6.3 nm	4.0%
MD κ^2 changed	0.66	0.72	5.3%
MD a changed	5.6 nm	5.8 nm	3.8%
MD all changed	See above	See above	2.8%

Model	Ideal value	MD value	Avg. rel. error
Ideal	-	-	7.5%
MD c changed	6.9 nm	4.0 nm	67.6%
MD κ^2 changed	0.66	0.77	6.7%
MD a changed	5.6 nm	5.0 nm	2.5%
MD all changed	See above	See above	69.2%

Model	Ideal value	MD value	Avg. rel. error
Ideal	-	-	14.5%
MD c changed	9.9 nm	10 nm	12.7%
MD κ^2 changed	0.66	0.61	16.6%
MD a changed	5.6 nm	5.0 nm	16.0%
MD all changed	See above	See above	14.9%

Model	Ideal value	MD value	Avg. rel. error
Ideal	-	-	14.4%
MD c changed	9.0 nm	7.7 nm	87.7%
MD κ^2 changed	0.66	0.57	15.4%
MD a changed	5.6 nm	5.7 nm	14.3%
MD all changed	See above	See above	72.0%

Figure S18: Comparison of MD *vs.* ideal values. Average relative change in the value of c, a, and κ^2 from the ideal to MD model in E_{ET} of **(a)** $Cy3_{(1)}\rightarrow Cy3.5_{(n)}$, **(b)** $Cy3_{(1)}\rightarrow AF647_{(n)}$, **(c)** $Cy3.5_{(1)}\rightarrow AF647_{(n)}$, and **(d)** $Cy3.5_{(1)}\rightarrow Cy5.5_{(n)}$.

The good agreements seen between experiment and simulation in **Figures 6c-f** are generally supportive of the idea that the MD simulations have allowed us to understand the system within a Förster description. On this basis we look for additional support that we are seeing sheet regime behavior, especially in the cases with 8 and 12 dyes where the E_{FRET} values rise to their highest values. In this regard it is worth examining the case of $Cy3.5_{(1)} \rightarrow Cy5.5_{(n)}$ (**Figure S14**) where the dyes are separated by two planes and which seems especially interesting in that the efficiency rise with added acceptors is exceptionally large being roughly a factor of 4. From the plot for position D1 in **Figure S14** we see that according to the MD simulation the D is on average about 7.8 nm from the central Cy5.5 A. Most other dyes are further away as one would expect if the A's were in their ideal positions within a plane, however, this is not true of the dyes in positions D7 and D6 that are added only in the cases with 8 or 12 A's. At higher number of dyes these high E_{FRET} outliers may have a greater probability and therefore weight in the system's ET.

Exploring the sheet aspect further, we recall that the sheet regime is favored by having small ratios of the intra-plane dye spacing's to the inter-plane spacing (a/c). Again this means the effect is greatest in the two-plane cases. DNA nanostructures systematically varying inter-plane spacing would require redesign of each individual block and, far more odiously, working with a different corresponding brick sequence set for every instance which would also require optimizing assembly in each case,[18-19] an undertaking vastly beyond the current scope, and so we turn to simulation using our validated MD-based model. In particular, we can perform new FRET simulations in which the fluctuating dye positions and orientations are again taken from the MD, but now add an arbitrary displacement of the D that moves it either closer to or further from the "plane" of A's. Performing such simulations for the one-plane $Cy3_{(1)} \rightarrow Cy3.5_{(n)}$ case and two-plane $Cy3.5_{(1)} \rightarrow Cy5.5_{(n)}$ case with 90% yield assumed (as in **Figure 6f**) and plotting the results as in **Figures 4b**, **S10**, we obtain **Figure S19**. That the curve for the two-plane dye arrangement is nearly linear and with a slope close to 4 strongly suggests that it is indeed in the sheet regime. The curve for the one-plane case instead shows substantial curvature, and the argument that this is in the sheet regime is not as conclusive.

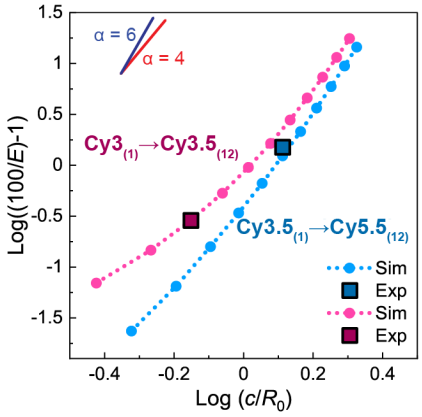

Figure S19: Experimental efficiencies *versus* MD-based FRET simulations. MD-based simulations of FRET efficiency for the indicated dye arrangements with the D position arbitrarily displaced and plotted in the format of **Figures 4b** and **S10** as a log-log plot. The nearly straight dashed red line with slope of approximately 4 indicates that $Cy3.5_{(1)}\rightarrow Cy5.5_{(12)}$ structure is in the sheet regime. The curvature of the blue line derived from simulations of $Cy3_{(1)}\rightarrow Cy3.5_{(12)}$ makes its regime less clear.

FRET efficiency in the fully dye-labeled block versus the pyramid configuration. Using the DNA block to organize the dyes in a pyramidal configuration is of interest because it provides 'focusing' which would be attractive if one wants not just efficiency, but efficiency in delivering energy to a particular nanoscale location. To quantify this effect, one can define the 'focusing ability' of the antenna as its E_{FRET} times the number of initial D's divided by the number of final A's. Using this measure, we find experimentally that the pyramidal design has about 3X the focusing ability of the full dye-labeled block (12/12) configuration. Thus it is just exactly the ratio of D's to A's, and this is surprising because it implies that the E_{FRET} of the two are about the same (as shown in **Figure 3e-f,h**). This is unexpected because the pyramidal arrangement will have (*i*) larger average distances between its initial D's and final A's due to its need for 'diagonal' transfers to get excitons in from the periphery, and (*ii*) reduced sheet enhancements in the downstream layers because they have fewer dyes. MD-based FRET simulation of these arguments are seen in **Figure S20** where the E_{ae} metric (Eq. S3) is plotted for the different configurations. Here we observe that the pyramid is indeed reduced being 24% below the 12/12 arrangement, and thus the focusing ability of the pyramid is "only" 2.4X times that of the 12/12 design. Also in accord with expectation is the role that homoFRET plays, as may be seen in **Figure S20** in the light pink points that were computed with homoFRET turned off. We observe that the pyramid result is more affected by the lack of homoFRET because the homoFRET aids the 'diagonal' transfers that are essential for the pyramid's focusing.

A final point concerns the unexpectedly high E_{FRET} of the pyramid that was observed in experiment despite the pyramid having one-third fewer dyes. Is there some gainful mechanism not captured in simulation that could conceivably benefit excitonic antenna design? To analyze this, it is important to notice that the simulations not only differ from experiment in proportion (pyramid *vs*. 12/12) but also in absolute magnitudes - the simulations in both cases over-estimate the experimental efficiencies by 30-40% (see **Figure S20**). Thus the simulations are missing some parasitic factor that is present in the experiments, and apparently this error is larger for the 12/12 design than for the pyramid.[20] An over-estimate of the efficiency by simulation was also observed in **Figure 6e** and this suggests the problem may be with the treatment of AF647, that perhaps it has some self-quenching that was not included in the simulation. Although there is evidence for somewhat unpredictable quenching of dyes by DNA bases,[21] it must remain speculative for now but would explain why the pyramid's relative efficiency was unexpectedly high - specifically, because the pyramid has fewer AF647 dyes. Under this interpretation, the pyramid is better only because it is more immune to the non-ideal dye,[3] and not because of some unknown enhancing mechanism that would be of greater interest.

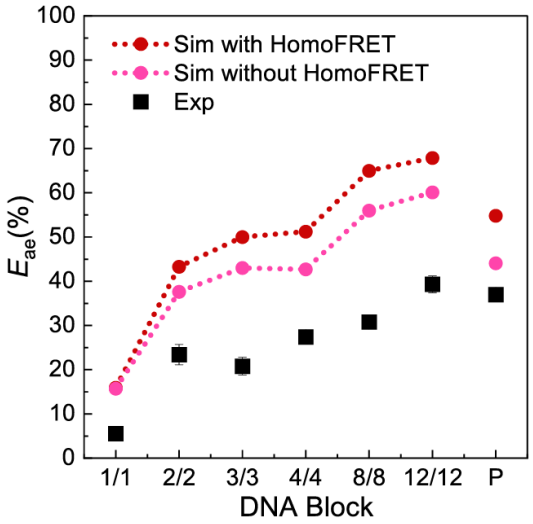

Figure S20: Comparison of the anywhere-to-end FRET efficiency as obtained experimentally and *via* MD-based simulation for the full 12/12 block and pyramidal design with and without homoFRET.

Supporting References:

1. Buckhout-White, S.; Spillmann, C. M.; Algar, W. R.; Khachatrian, A.; Melinger, J. S.; Goldman, E. R.; Ancona, M. G.; Medintz, I. L. Assembling Programmable FRET-Based Photonic Networks Using Designer DNA Scaffolds. *Nat. Comm.* **2014,** *5*, 5615.

2. Diaz, S. A.; Buckhout-White, S.; Ancona, M. G.; Spillmann, C. M.; Goldman, E. R.; Melinger, J. S.; Medintz, I. L. Extending DNA-Based Molecular Photonic Wires with Homogeneous Forster Resonance Energy Transfer. *Adv. Opt. Mater.* **2016,** *4*, 399-412.

3. Klein, W. P.; Rolczynski, B. S.; Oliver, S. M.; Zadegan, R.; Buckhout-White, S.; Ancona, M. G.; Cunningham, P. D.; Melinger, J. S.; Vora, P. M.; Kuang, W.; Medintz, I. L.; Díaz, S. A. DNA Origami Chromophore Scaffold Exploiting HomoFRET Energy Transport to Create Molecular Photonic Wires. *ACS Appl. Nano Mater.* **2020,** *3*, 3323-3336.

4. Spillmann, C. M.; Ancona, M. G.; Buckhout-White, S.; Algar, W. R.; Stewart, M. H.; Susumu, K.; Huston, A. L.; Goldman, E. R.; Medintz, I. L. Achieving Effective Terminal Exciton Delivery in Quantum Dot Antenna-Sensitized Multistep DNA Photonic Wires. *ACS Nano* **2013,** *7*, 7101-18.

5. Klein, W. P.; Díaz, S. A.; Buckhout-White, S.; Melinger, J. S.; Cunningham, P. D.; Goldman, E. R.; Ancona, M. G.; Kuang, W.; Medintz, I. L. Utilizing HomoFRET to Extend DNA-Scaffolded Photonic Networks and Increase Light-Harvesting Capability. *Adv. Opt. Mater.* **2017,** *6*.

6. Olejko, L.; Bald, I. FRET Efficiency and Antenna Effect in Multi-Color DNA Origami-Based Light Harvesting Systems. *RSC Adv.* **2017,** *7*, 23924-23934.

7. Bosch, C. D.; Jevric, J.; Burki, N.; Probst, M.; Langenegger, S. M.; Haner, R. Supramolecular Assembly of DNA-Phenanthrene Conjugates into Vesicles with Light-Harvesting Properties. *Bioconjug. Chem.* **2018,** *29*, 1505-1509.

8. Kownacki, M.; Langenegger, S. M.; Liu, S. X.; Haner, R. Integrating DNA Photonic Wires into Light-Harvesting Supramolecular Polymers. *Angew. Chem. Int. Ed.* **2019,** *58*, 751-755.

9. Douglas, S. M.; Marblestone, A. H.; Teerapittayanon, S.; Vazquez, A.; Church, G. M.; Shih, W. M. Rapid Prototyping of 3D DNA-Origami Shapes with CaDNAno. *Nucleic Acids Res.* **2009,** *37*, 5001-6.

10. Wang, V.; Ermann, N.; Keyser, U. F. Current Enhancement in Solid-State Nanopores Depends on Three-Dimensional DNA Structure. *Nano Lett.* **2019,** *19*, 5661-5666.

11. Fischer, S.; Hartl, C.; Frank, K.; Radler, J. O.; Liedl, T.; Nickel, B. Shape and Interhelical Spacing of DNA Origami Nanostructures Studied by Small-Angle X-Ray Scattering. *Nano Lett.* **2016,** *16*, 4282-7.

12. Pettersen, E. F.; Goddard, T. D.; Huang, C. C.; Couch, G. S.; Greenblatt, D. M.; Meng, E. C.; Ferrin, T. E. UCSF Chimera--A Visualization System for Exploratory Research and Analysis. *J. Comput. Chem.* **2004,** *25*, 1605-12.

13. Van Der Spoel, D.; Lindahl, E.; Hess, B.; Groenhof, G.; Mark, A. E.; Berendsen, H. J. GROMACS: Fast, Flexible, and Free. *J. Comput. Chem.* **2005,** *26*, 1701-18.

14. Hornak, V.; Abel, R.; Okur, A.; Strockbine, B.; Roitberg, A.; Simmerling, C. Comparison of Multiple AMBER Force Fields and Development of Improved Protein Backbone Parameters. *Proteins* **2006,** *65*, 712-25.

15. Wang, J.; Wolf, R. M.; Caldwell, J. W.; Kollman, P. A.; Case, D. A. Development and Testing of a General AMBER Force Field. *J. Comput. Chem.* **2004,** *25*, 1157-74.

16. Mark, P.; Nilsson, L. Structure and Dynamics of the TIP3P, SPC, and SPC/E Water Models at 298 K. *J. Phys. Chem. A* **2001,** *105*, 9954-9960.

17. Mathur, D.; Kim, Y. C.; Díaz, S. A.; Cunningham, P. D.; Rolczynski, B. S.; Ancona, M. G.; Medintz, I. L.; Melinger, J. S. Can a DNA Origami Structure Constrain the Position and Orientation of an Attached Dye Molecule? *J. Phys. Chem. C* **2020**, *125*, 1509-1522.

18. Ke, Y.; Ong, L. L.; Shih, W. M.; Yin, P. Three-Dimensional Structures Self-Assembled from DNA Bricks. *Science* **2012,** *338*, 1177-83.

19. Ong, L. L.; Hanikel, N.; Yaghi, O. K.; Grun, C.; Strauss, M. T.; Bron, P.; Lai-Kee-Him, J.; Schueder, F.; Wang, B.; Wang, P.; Kishi, J. Y.; Myhrvold, C.; Zhu, A.; Jungmann, R.; Bellot, G.; Ke, Y.; Yin, P. Programmable Self-Assembly of Three-Dimensional Nanostructures from 10,000 Unique Components. *Nature* **2017,** *552*, 72-77.

20. Diaz, S. A.; Oliver, S. M.; Hastman, D. A.; Medintz, I. L.; Vora, P. M. Increased Transfer Efficiency from Molecular Photonic Wires on Solid Substrates and Cryogenic Conditions. *J. Phys. Chem. Lett.* **2018,** *9*, 3654-3659.

21. Seidel, C. A. M.; Schulz, A.; Sauer, M. H. M. Nucleobase-Specific Quenching of Fluorescent Dyes. 1. Nucleobase One-Electron Redox Potentials and Their Correlation with Static and Dynamic Quenching Efficiencies. *J. Phys. Chem.* **1996,** *100*, 5541-5553.